

# Towards single-electron metrology

Karsten Flensberg\*

*Danish Institute of Fundamental Metrology,  
Anker Engelunds Vej 1, DK-2800 Lyngby, Denmark*

and

Arkadi A. Odintsov\*\*

*Nederlands Meetinstituut, P.O. Box 654, 2600 AR Delft, The Netherlands, and  
Department of Applied Physics, Delft University of Technology, 2628 CJ Delft, The  
Netherlands,*

and

Feike Liefink and Paul Teunissen

*NMi Van Swinden Laboratorium, P.O. Box 654, 2600 AR Delft, The Netherlands.*

21 December, 1998.

We review the status of the understanding of single-electron transport (SET) devices with respect to their applicability in metrology. Their envisioned role as the basis of a high-precision electrical standard is outlined and is discussed in the context of other standards. The operation principles of single electron transistors, turnstiles and pumps are explained and the fundamental limits of these devices are discussed in detail. We describe the various physical mechanisms that influence the device uncertainty and review the analytical and numerical methods needed to calculate the intrinsic uncertainty and to optimise the fabrication and operation parameters. Recent experimental results are evaluated and compared with theoretical predictions. Although there are discrepancies between theory and experiments, the intrinsic uncertainty is already small enough to start preparing for the first SET-based metrological applications.

## Contents

<b>1</b>	<b>Introduction</b>	<b>3</b>
1.1	General introduction . . . . .	3
1.2	Historic framework . . . . .	4
1.3	Metrological motivation for SET research . . . . .	5
1.4	Basic requirement for the Coulomb blockade of tunneling . . . . .	7
1.5	The SET transistor . . . . .	9
1.5.1	Properties of the SET transistor . . . . .	9
1.5.2	Applications of the SET transistor . . . . .	10
1.6	Single-electron pumps and turnstiles . . . . .	11
1.6.1	The electron pump . . . . .	12
1.6.2	The turnstile . . . . .	13
<b>2</b>	<b>Experimental status of pumps and turnstiles</b>	<b>15</b>
2.1	Fabrication technique . . . . .	15
2.2	Uncertainty . . . . .	17
<b>3</b>	<b>Error mechanisms</b>	<b>18</b>
3.1	Cycle missing . . . . .	19
3.2	Thermally activated errors . . . . .	19
3.3	Cotunneling . . . . .	20
3.4	Photon assisted tunneling . . . . .	22
3.5	Background charges . . . . .	23
<b>4</b>	<b>Numerical analysis of single electron devices</b>	<b>23</b>
4.1	Methods and tools for numerical analysis . . . . .	23
4.2	SENECA: a global approach to rare events . . . . .	24
4.3	Results of simulations . . . . .	25
<b>5</b>	<b>Comparison of theory and experiments</b>	<b>29</b>
5.1	Discrepancies between measured and predicted errors . . . . .	29
5.2	Possible sources of additional error mechanisms . . . . .	31
<b>6</b>	<b>Alternative designs for single-electron current standards</b>	<b>31</b>
6.1	Surface acoustic waves as carriers of single electrons . . . . .	32
6.2	Phase locking of coherent Cooper pair tunneling . . . . .	33
6.3	Electron counting by a high-speed electrometer . . . . .	34
<b>7</b>	<b>Conclusions</b>	<b>34</b>
<b>8</b>	<b>Acknowledgments</b>	<b>35</b>

# 1 Introduction

## 1.1 General introduction

In recent years, the development of sub-micron devices has offered the opportunity to transport electric charge by the manipulation of individual electrons. Devices have been fabricated that can be controlled by an externally applied alternating signal in such a way, that an integer number of electron charges is transferred through the device per cycle. Once the frequency of the external signal is accurately known, the current through the device can, in principle, be calculated with high precision. Such single-electron transport (SET) devices have opened the path towards the realization of high-precision current and capacitance standard. A high-precision current standard is needed because a standard for the unit of electrical current, the ampere, is presently not available in a direct and accurate manner, although it is one of the base units of the International System of Units (SI). The construction of a high-precision capacitance standard using SET devices offers a realistic alternative for the calculable capacitor. In general, there is also a growing need in science and industry to measure very low current levels with high precision, driven by the ongoing tendency towards miniaturization of electrical circuits.

The basis of high-precision current and capacitance standards that are presently being developed, is formed by sub-micron devices like turnstiles and pumps. In practice the observed intrinsic uncertainty of these devices is of the order of 1 part in  $10^8$ , already approaching the uncertainty levels of Josephson voltage standards and quantum Hall resistance standards. Theoretically, SET devices are capable to individually transfer electrons with an error per electron that is much smaller. This discrepancy is caused by yet unknown mechanisms.

Because of the extremely difficult and failure-sensitive fabrication process of SET devices and because of the ultra-low temperatures needed for their operation, research on SET devices is inherently time and money consuming. An efficient feedback between experimental results and theoretical understanding is necessary to improve the effectiveness of the research activities. For that reason, an overview is desired of today's understanding of the properties of SET devices when applied within metrology.

The focus will be on SET transistors, and turnstile and pump devices. Their working principle will be discussed in the first section of this article. A brief introduction to the fabrication technique and a short overview of the experimental status are given in Sec. 2. In Sec. 3 and 4 it will be shown that the error mechanisms affecting the accuracy of SET devices are in general reasonably well understood and that theoretical calculations can support the design of new device lay-outs. Nevertheless, in Sec. 5 attention is paid to the fact that in many cases the experimentally observed uncertainties are still much higher than expected from theory. Finally, in Sec. 6 some alternative devices are briefly discussed, such as the recently developed devices that make use of surface acoustic waves.

Nowadays SET devices are able to accurately generate currents at the level of 1 pA. This is already high enough to realize a capacitance standard. Such standard is based on charging a capacitor of typically 1 pF with an accurately known number of electrons and subsequently measuring the voltage that has developed across the capacitor. However, the 1 pA level is still too low to accurately calibrate current sources which operate at higher, more convenient levels (microamperes and higher). One of the major tasks within SET metrology is to increase the amplitude of the current that can be generated by SET devices, while maintaining a very low uncertainty. This article is meant to serve as a useful

reference in that process.

## 1.2 Historic framework

The phenomenon of the Coulomb blockade of tunneling provides the possibility to control the transport of individual electrons. The Coulomb blockade can be understood from Fig. 2 which shows two conducting electrodes coupled to a small island via tunnel junctions. Transport of electrons from one electrode to the other can take place by means of tunneling through the junctions. However, when the total capacitance  $C_\Sigma$  of the island is sufficiently small, the energy  $E_C = e^2/2C_\Sigma$  (with  $e$  the electron charge) needed to charge the island with an extra electron becomes high enough to prohibit the tunneling of other electrons. The Coulomb blockade of tunneling can only be observed at low temperatures  $k_B T \ll E_C$ , at which thermally activated transport is suppressed (here  $k_B$  is Boltzmann's constant).

The Coulomb blockade was for the first time experimentally observed in disordered granular materials [1]. Later, techniques were developed to fabricate — in a controlled way — ultra-small tunnel junctions that exhibit the Coulomb blockade effect [2]. Nowadays these junctions form the basis of so-called single electron tunneling (SET) devices, in which the transport of individual electrons can be controlled by means of externally applied signals. Likharev *et al.* pointed out [3] the possibility to use these devices for metrological applications such as an electrical current standard, for which the magnitude of the generated current is determined by the frequency  $f_{\text{SET}}$  of the externally applied signal and the number  $k$  of electrons that is transferred per period:

$$I_{\text{SET}} = k e f_{\text{SET}}. \quad (1)$$

The initial suggestion was to pass a current through a single tunnel junction and to lock the rate  $I_{\text{SET}}/e$  to an external ac source. The experiments however showed that the Coulomb blockade and consequently the sought SET oscillations for a single junction are strongly suppressed [4]. This is attributed to quantum charge fluctuations in the electromagnetic surroundings [5, 6, 7, 8].

Special precautions have been taken in several experiments to suppress quantum fluctuations by attaching highly resistive leads to the junctions [9, 10, 11]. Effective shielding from external quantum fluctuations can also be achieved by placing several tunnel junctions in series. In this way SET oscillations were experimentally observed in the form of current plateaux in the current-voltage characteristics of tunnel junction arrays irradiated by a microwave signal [12]. However, the flatness of the plateaux was still poor.

Devices to manipulate electrons in a more controlled way were developed, starting with the so-called single electron turnstile [13]. A slightly more complicated device is the single-electron pump, in which electrons are moved through a series of tunnel junctions without applying a bias voltage [14]. The first high-accuracy pump was fabricated at the National Institute of Standards and Technology (NIST) using a 5-junction design [15]. Recently, an improved 7-junction device was fabricated and studied, and an error per pumped electron of 1 part in  $10^8$  was achieved [16, 17, 18]. This accuracy is still much lower than theory predicts on the basis of the present understanding of error mechanisms. Further research is therefore still necessary. Nevertheless, the achieved accuracy already corresponds to the required level for the construction of a new high accuracy capacitance standard proposed in Ref. [19].

Superconducting devices have also been proposed as a candidate to relate current to frequency [20]. Frequency locking at  $I = 2ef$  has been observed in small superconducting

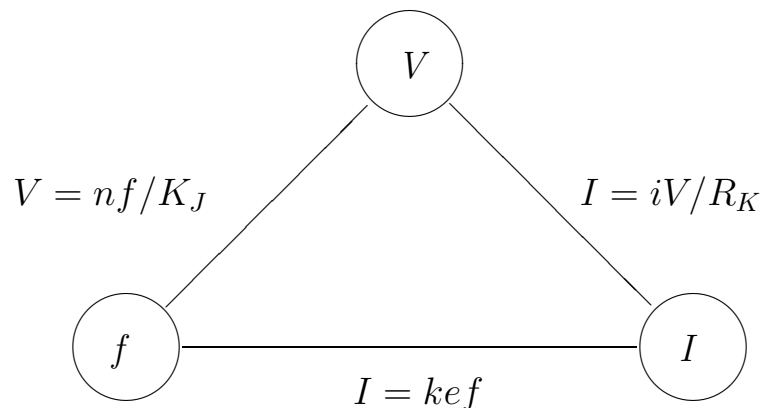


Figure 1: The metrological triangle connecting frequency, voltage and current through the Josephson effect, the quantum-Hall effect and the single-electron tunneling effect. Here  $i, n$  and  $k$  are integers and  $R_K = h/e^2$  and  $K_J = h/2e$ .

Josephson junctions (see [21, 22] and references therein), but the effect was strongly suppressed by thermal smearing and quantum fluctuations [23, 24]. Like in the normal metal case, it is necessary to consider arrays of junctions in order to eliminate the quantum fluctuations [25].

Very recently, a device was developed at Cambridge University that utilizes a surface acoustic wave (SAW) to pass electrons through a quantum point contact in the pinch-off regime [26, 27]. The electric field induced by the SAW leads to the formation of quantum dots which move along the constriction transporting an integer number of electrons per period of the SAW. The first results are encouraging, but much improvement is needed to achieve an uncertainty comparable to that of a SET pump.

### 1.3 Metrological motivation for SET research

The metrological motivation for research on SET devices lies in their expected applicability in current standards and capacitance standards.

A current standard based on the manipulation of single electrons will be the first direct and accurate representation of the ampere. Presently the ampere, being the (only) electrical base unit within the SI, is represented by the combination of the Josephson-array voltage standard and quantized Hall resistance standard through Ohm's law. This is an indirect and cumbersome method and in practice only secondary standards for voltage and resistance are combined in this way.

A SET current standard will not be a *realisation* of the ampere in the sense that it is a reconstruction according to the present SI definition, because the basis for this definition is Ampere's law, which expresses the force generated by two currents. Ampere's law thus connects the electrical and mechanical units within the SI system. Using force measurements to realise the ampere is, however, not very practical. A far more convenient way appeared to be the application of Ohm's law and to combine voltage and resistance standards. In 1990 it was agreed that the quantum-Hall effect and the Josephson effect are representations of the volt and ohm, respectively. The assignments of values of the new quantum standards were done by experiments where, e.g., the Josephson voltage was measured in terms of mechanical units. The resulting relative uncertainties are of the order  $10^{-7}$ , which is much larger than the reproducibility of the Josephson voltage standards,

which is of the order  $10^{-9}$ . The search towards a SET current standard can therefore also be viewed in a broader perspective, namely to bring up arguments for a redefinition of the SI system, where the electrical units are *defined* in terms of quantum standards, and mechanical units are being *derived* from those.

Presently, it is possible to make an accurate SET current standard only for small current values, typically a few picoampere. The uncertainty of the current is dominated by the uncertainty in the average number  $k$  of electrons that is transferred per cycle of the drive frequency  $f_{\text{SET}}$ . For a SET standard that can be accurately linked to secondary standards, the current level has to be increased by at least several orders of magnitude. However, simply increasing the current by means of increasing  $f_{\text{SET}}$  is not a solution since this would rapidly increase the relative uncertainty (see Sec. 3). It is an inherent drawback of nowadays current standards that are based on SET devices.

A capacitance standard based on SET devices does not need currents higher than a few picoampere, in contrast to a current standard. For an application in capacitance standards, the SET device is used to charge a capacitor with an accurately known number of electrons [28, 19]. By measuring the voltage that consequently develops across the capacitor, the zero-frequency capacitance value can be determined. Again, the uncertainty of measurement is dominated by the uncertainty in the average number  $k$  of electrons that is transferred per cycle of the drive frequency  $f_{\text{J}}$ . It is expected that capacitance measurements can be carried out with relative uncertainties of  $10^{-7}$  at 1 pF [29].

Besides their potential usefulness as measurement standards for calibration of current and capacitance, SET devices can also be exploited for fundamental metrology experiments, such as an alternative determination of the value of the electron charge. One way of doing this is to use Ohm's law by passing a SET current through a quantized Hall device while comparing the Hall voltage with a Josephson-array voltage standard. This closes the so-called quantum metrological triangle, Fig. 1, first suggested by Likharev and Zorin [20].

The quantized Hall resistance  $R$  and the Josephson voltage  $V$  are given by

$$V = nf_{\text{J}}/K_{\text{J}}, \quad R = R_{\text{K}}/i, \quad (2)$$

where  $n$  and  $i$  are integers, and  $f_{\text{J}}$  is the drive frequency of the Josephson-array voltage standard. The constants of proportionality  $K_{\text{J}}$  and  $R_{\text{K}}$  are called the Josephson constant and the Von Klitzing constant, respectively. Practical values for  $K_{\text{J}}$  and  $R_{\text{K}}$  have been recommended to facilitate the international comparison of voltage and resistance measurements[30]. The recommended values are denoted by  $K_{\text{J}-90}$  and  $R_{\text{K}-90}$ , respectively. By combining Eqs. (1) and (2) and inserting values for  $K_{\text{J}}$  and  $R_{\text{K}}$ , a value for the electron charge can be calculated from

$$e = \left( \frac{f_{\text{J}}}{f_{\text{SET}}} \right) \times \left( \frac{nk}{i} \right) \times \left( \frac{1}{R_{\text{K}}K_{\text{J}}} \right). \quad (3)$$

Of course, this value has to be consistent with earlier determinations of  $e$ . Based on the physical understanding of the Josephson effect and the quantum Hall effect, the constants  $K_{\text{J}}$  and  $R_{\text{K}}$  are predicted to be combinations of  $e$  and  $h$ ,

$$K_{\text{J}} = \frac{2e}{h}, \quad R_{\text{K}} = \frac{h}{e^2}. \quad (4)$$

This means that, in addition, the value for  $f_{\text{J}}/f_{\text{SET}} \times nk/i$  is expected to be exactly equal to 2. It should be stressed that a comparison of the so measured value of  $e$  with the

already known value of  $e$  does not yield any additional information about the values of the fundamental constants, or the correctness of the underlying theory. It merely provides a useful consistency check, unfortunately without providing a clue with respect to the source of the possible inconsistencies.

In a more direct way, the electron charge can be measured by charging a capacitor  $C_s$  with an accurately known number  $m$  of electrons, using a SET current source. When the value of the capacitor is accurately known, through traceability towards the calculable capacitor, and by measuring the voltage across the capacitor using a Josephson standard, the value of  $e$  can be calculated from

$$e = \left(\frac{n}{m}\right) \times \left(\frac{C_s f_J}{K_J}\right). \quad (5)$$

Again, this value must be consistent with the generally accepted value for the electron charge. Alternatively this method of charging a capacitor can be used for a determination of the fine structure constant  $\alpha$  [19], which is defined by

$$\alpha \equiv \frac{\mu_0 c e^2}{h}, \quad (6)$$

where  $\mu_0$  is the permeability of vacuum and  $c$  is the velocity of light. Combining Eqs. (5) and (6) the value for  $\alpha$  is given by

$$\alpha = \left(\frac{\mu_0 c}{2}\right) \times \left(\frac{n}{2m}\right) \times f_J C_s. \quad (7)$$

Such a determination of  $\alpha$  would be helpful in the field of fundamental constants.

#### 1.4 Basic requirement for the Coulomb blockade of tunneling

The Coulomb blockade of tunneling can only be observed if the number of electrons on each island is well defined. First of all, this implies that the energy needed to place an additional charge on an island must be large compared to the energy related to thermal fluctuations:

$$E_C = e^2/2C_\Sigma \gg k_B T, \quad (8)$$

where  $C_\Sigma$  is the total capacitance of the island. Secondly, quantum fluctuations must be suppressed. In other words, the wave function of an electron should be localized on a single island. Therefore, the energy uncertainty associated with the lifetime  $R_T C$  due to tunneling of electrons across the junction (with capacitance  $C$  and tunneling resistance  $R_T$ ) must be much smaller than  $E_C$ . From this follows:

$$R_T \gg h/e^2 \simeq 25.8 \text{ k}\Omega, \quad (9)$$

where  $h$  is Planck's constant.

The latter condition suggests that the larger the tunneling resistance the better. This is unfortunately not the case, because the speed of operation is limited by the time  $R_T C$ , which therefore should be as short as possible. One thus has to find an optimum choice of  $R_T$  which compromises between speed and leakage.

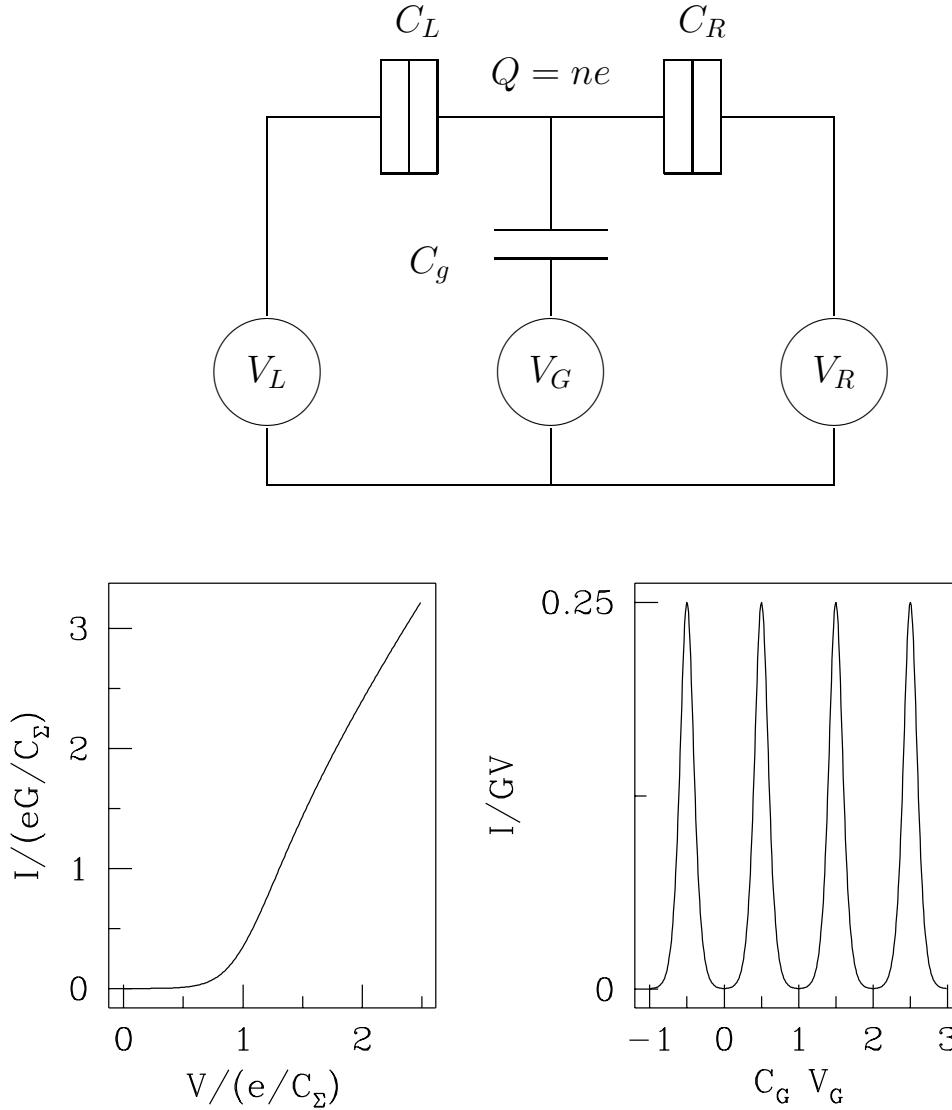


Figure 2: SET transistor. The top panel shows a diagram of a SET transistor with a metallic island which is connected to the external electrodes through two tunnel junctions (represented by boxes). The capacitances of the tunnel junctions are  $C_L$  and  $C_R$ . The lower left panel shows the calculated current-voltage characteristic at low temperature ( $T = E_C/10$ ) and  $V_G = 0$ . For a bias voltage above threshold,  $V_{tr} = e/C_\Sigma$ , the current can flow, whereas for smaller bias voltage, the current is blocked. The number of electrons on the island can be tuned by the gate voltage  $V_G$ . The properties of the transistor change periodically with the gate voltage  $V_G$ . The period corresponds to addition of one electron to the island. This is shown in the lower right panel, where the conductance is plotted versus  $V_G$ . The current reaches a maximum each time the charge state with  $N$  electrons has the same energy as the state with  $N + 1$  electrons.

## 1.5 The SET transistor

### 1.5.1 Properties of the SET transistor

To elucidate the effect of the Coulomb blockade on the electric properties of nanometer scale devices we consider the so-called single electron transistor whose diagram is shown in the upper part of Fig. 2. The central island can only be occupied by an integer number of electrons, provided that the conditions (8), (9) are fulfilled. By applying a bias voltage ( $V_L - V_R$ ) and changing the potential  $V_G$  of the gate electrode the number of electrons on the island can be changed. If  $V_G$  is adjusted such that the charging energy, needed to add (remove) an electron to (from) the central island, is larger than the applied bias voltage and the thermal energy, current through the structure is blocked. If however the potentials are selected so that the charging energy is zero, current can flow. The device thus acts like a transistor where a small change in offset charge on the gate capacitor changes the state of the device from closed to opened. For comprehensive reviews of the Coulomb blockade see e.g. Refs. [3, 31].

The electrostatics of the system is determined by the external voltages and the charge,  $Q = Ne$ , on the central island. The part of the total electrostatic energy which depends on the number of electrons is

$$E_{\text{el}} = \frac{(Q - Q_{\text{ex}})^2}{2C_{\Sigma}}, \quad (10)$$

where the total capacitance of the island is  $C_{\Sigma} = (C_L + C_R + C_G)$  and the induced charge on the island is defined as  $Q_{\text{ex}} = (V_L C_L + V_R C_R + V_G C_G)$ . The charging energies for adding ( $\Delta^+$ ) or removing ( $\Delta^-$ ) an electron from the island are given by

$$\Delta^{\pm} = E_{\text{el}}(Q) - E_{\text{el}}(Q \pm e) = \mp \frac{e}{C_{\Sigma}} \left( Q - Q_{\text{ex}} \pm \frac{e}{2} \right). \quad (11)$$

Thus if  $Q_{\text{ex}} = (n + \frac{1}{2})e$  the two charge states  $Q = ne$  and  $Q = (n + 1)e$  have the same energy. As a result, current can flow freely because the system can alternate between the two degenerate states. Away from this degeneracy point the current is blocked as long as  $e(V_L - V_R) \ll e^2/2C_{\Sigma}$  and  $k_B T \ll e^2/2C_{\Sigma}$ .

The junctions in a SET transistor normally consist of two layers of metal (usually Al) separated by thin insulating barrier (Al oxide). The overlap of the initial and final electron states  $|i\rangle$  and  $|f\rangle$  on the two sides of the barrier is described by the tunneling Hamiltonian,

$$\hat{V} = \sum_{i,f} T_{f,i} |f\rangle \langle i|, \quad (12)$$

where  $T_{f,i}$  is the transition probability from state  $|i\rangle$  to state  $|f\rangle$ . Fermi's golden rule allows one to evaluate the rate  $\Gamma_{if}$  of tunneling from state  $|i\rangle$  to state  $|f\rangle$ ,

$$\Gamma_{if} = \frac{2\pi}{\hbar} \left| \langle f | \hat{V} | i \rangle \right|^2 \delta(E_f - E_i), \quad (13)$$

Using these formulae, we can find the electron tunneling rates through the left and right junctions in Fig. 2,

$$\Gamma_{L,R}(Q \rightarrow Q \pm e) = \frac{1}{e^2 R_{T(L,R)}} \frac{\Delta^{\pm}}{1 - \exp(-\Delta^{\pm}/k_B T)} \quad (14)$$

where  $R_{T(L,R)} = \hbar/2\pi e^2 |T_{L,R}|^2 N_F^2$  are the nominal tunneling resistances of the junctions and  $N_F$  is the density of states at the Fermi level. From Eq. (14) we see that tunneling

is exponentially suppressed if the electrostatic energy after the tunnel event is larger than before (i.e.  $\Delta^\pm < 0$ ).

It is important to realize that the tunneling rate, given by Eq. (14), relies on the assumption that electrostatic equilibrium is restored instantaneously after a tunneling event. In terms of time scales this is true if the characteristic time for redistribution of the charge, which is the inverse plasma frequency, is much shorter than the “tunneling time”  $\hbar/\Delta$ . This assumption is sometimes called the capacitance model (which corresponds to the “global rule” in Ref. [31]) and it is certainly a valid approximation for good metal conductors.

The dynamic properties of a SET transistor are determined by the tunneling rates (14), and can be described by the master equation

$$\frac{d}{dt}P(Q, t) = \sum_{\pm} [P(Q \pm e, t)\Gamma(Q \pm e \rightarrow Q) - P(Q, t)\Gamma(Q \rightarrow Q \pm e)], \quad (15)$$

where  $\Gamma = \Gamma_L + \Gamma_R$  is the sum of the tunneling rates through both junctions and  $P(Q)$  is the probability of the charge state  $Q$ . In a steady state ( $dP(Q, t)/dt = 0$ ) there is a balance between the number of electrons entering and leaving the island so that the probability of a transition from the state  $Q$  to the state  $Q + e$  is equal to the probability of a transition in the opposite direction. Thus it follows that

$$P(Q)\Gamma(Q \rightarrow Q + e) = P(Q + e)\Gamma(Q + e \rightarrow Q). \quad (16)$$

This equation yields  $P(Q)$  and once that is found the current is given by

$$I = e \sum_Q P(Q) [\Gamma_L(Q \rightarrow Q + e) - \Gamma_L(Q \rightarrow Q - e)]. \quad (17)$$

In the lower part of Fig. 2 we illustrate the behavior of the single electron transistor by plotting the characteristics based on the solution of Eq. (16). The source-drain conductance depends strongly on the additional charge on the island induced by the gate voltage. The distance between two conductance minima corresponds to the addition of one electron charge to the island. Clearly, a SET transistor is a very sensitive detector of electric charge.

### 1.5.2 Applications of the SET transistor

Since the source-drain conductance of a SET transistor is strongly dependent on the induced charge on the island it is possible to use the SET transistor as a very sensitive detector of changes in gate voltage [32, 33]. This can be done by applying a suitable bias current and by measuring the dependence of the source-drain voltage  $V_{SD}$  as a function of the gate voltage  $V_G$ . After optimisation of the values of the junction capacitances and gate capacitance a voltage gain  $dV_{SD}/dV_G$  close to one can be obtained. This electrometer operation of the SET transistor however only works at low frequencies due to inevitable stray capacitances. The low-frequency properties are strongly influenced by noise sources inside and close to the tunnel junctions. These sources give rise to a  $1/f$  - like background charge noise on the gate electrode with a magnitude of typically  $10^{-4} e/\sqrt{\text{Hz}}$  at 10 Hz. This will be discussed in Sec. 3.5.

The advantage of a SET electrometer over conventional electrometers is their very low leakage. If the role of stray capacitances can be minimized, SET electrometers are

especially useful when applied as a null detector in the experiment of charging a cryogenic capacitor using a SET electron pump [19]. This was first shown theoretically in Ref. [34] and has recently been confirmed experimentally [17]. Another application of a SET transistor is as a non-invasive probe of the local chemical potential in two-dimensional electron gas systems [38, 39].

The electrometer operation of the single-electron transistor however only works at low frequencies due to the parasitic lead capacitances which limits speed. For higher operation speed an on-chip amplifier is necessary. However recently a new method was developed to avoid this drawback. Schoelkopf *et al.* [40] have demonstrated a combination of a SET transistor and a radio frequency resonant circuit, a so-called RF-SET device. The SET transistor was used to modify the damping of the resonant circuit (a similar principle is used in RF SQUIDS). This RF-SET device has a charge sensitivity of the order  $10^{-5} e/\sqrt{\text{Hz}}$  at 1 MHz, which no doubt will open for new areas of application of single-electron electrometers, see also Sec. 6.3.

Pekola *et al.* showed that a SET transistor can be utilized as a thermometer [41, 42]. The idea is to use the thermal smearing of the Coulomb gap in the current-voltage characteristics as a measure of temperature. In contrast to other single-electron devices, such a thermometer can operate at temperatures somewhat larger than the temperature corresponding to the Coulomb charging energy. The advantage of the SET based thermometer is its insensitivity magnetic fields, unlike other cryogenic thermometers. In fact this thermometer measures directly the ratio of temperature to voltage.

Recent technological advances in fabrication have resulted in a SET transistor positioned at the end of a sharp glass tip [35]. Such a single-electron scanning electrometer (SETSE) is capable of mapping static electric fields and charges with a spatial resolution of 100 nm and a charge sensitivity of a small fraction of an electron charge. The SETSE has been used to image and measure depleted regions, local capacitance, band bending, and contact potentials on the surface of semiconductor samples. Another application of a SET transistor is as a non-invasive probe of the local chemical potential in two-dimensional electron gas systems [38, 39].

## 1.6 Single-electron pumps and turnstiles

Single-electron pumps and turnstiles are devices that generate a dc current satisfying the fundamental relation (1) with high accuracy. They consist of a series of tunnel junctions in which the electric potential of the islands are manipulated such that only one electron is transferred through the device per cycle of an externally applied signal. The general layout for both devices is shown in Fig. 3. The islands with charges  $Q_1, \dots, Q_n$  ( $Q_i = N_i e$ ) are separated by tunnel junctions with capacitances  $C_1, \dots, C_{n+1}$ . The electric potential of each island can be controlled by the gate voltages  $V_{G1}, \dots, V_{Gn}$  through the gate capacitances  $C_{G1}, \dots, C_{Gn}$ .

The dynamics of such a device can be described by a master equation for the probabilities  $P(\mathbf{Q}, t)$  of the charge states  $\mathbf{Q} = (Q_1, \dots, Q_n)$  of the system [43, 44, 45], which is a generalisation of Eq. (15) for the non-stationary case

$$\frac{d}{dt}P(\mathbf{Q}, t) = \sum_{\mathbf{Q}'} [P(\mathbf{Q}', t)\Gamma(\mathbf{Q}' \rightarrow \mathbf{Q}) - P(\mathbf{Q}, t)\Gamma(\mathbf{Q} \rightarrow \mathbf{Q}')]. \quad (18)$$

The first term comes from tunneling *into* the charge state  $\mathbf{Q}$  with a rate  $\Gamma(\mathbf{Q}' \rightarrow \mathbf{Q})$  whereas the second term is due to tunneling *out of* this state with a rate  $\Gamma(\mathbf{Q} \rightarrow \mathbf{Q}')$ . The

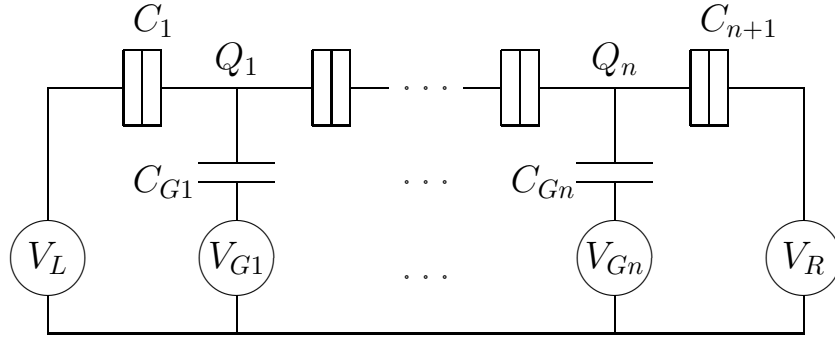


Figure 3: Principle of pump. A series of islands  $i = 1, \dots, n$ , with charges  $Q_i$ , are connected by tunnel junctions and coupled through capacitances  $C_{G_i}$  to gate voltages. These gate voltages control the charges on the islands. By suitable periodic variations of the gate voltages a well-defined number of electrons can be transferred through the device. The turnstile has a finite voltage drop across the array, and typically only one time-dependent gate voltage is applied to the central island. The pump usually operates without a dc bias.

tunneling rates  $\Gamma$  are time dependent if  $\Delta^\pm$  is time dependent, see Eq. (14). Numerical simulations based on this master equation are reviewed in Sec. 4.

Notice that we described the single-electron tunneling process in terms of the orthodox rate equation (18), which assumes thermalization of the system between each tunneling event. If the system does not have time to equilibrate between tunneling events the non-equilibrium distribution of the electron system has to be taken into account. This has been considered in Refs. [36, 37].

### 1.6.1 The electron pump

The simplest electron pump contains two islands ( $n = 2$ ) and three tunnel junctions (see Fig. 3). By changing the gate potentials  $V_{G_1}$  and  $V_{G_2}$  the charge configuration  $\mathbf{Q} = (Q_1, Q_2)$  can be controlled. Pump operation starts by increasing the potential of the island "1" such that an electron tunnels onto this island from the left electrode. Then the potential of the island "1" is lowered again, while simultaneously increasing the potential of the island "2". This results in tunneling of an electron from the island "1" to the island "2". Finally, by lowering the potentials of both islands, an electron from the island "2" will be forced to tunnel to the right electrode. The device has then returned to its initial charge state and one electron has been pumped from left to right. Typical cycling rates are in the range of a few megahertz, i.e. RF frequencies, corresponding to currents of the order of a picoampere. For optimal performance the bias voltage ( $V_L - V_R$ ) must be near zero.

One can illustrate the pump operation by means of the diagram in Fig. 4, which displays the regions of minimum Coulomb energy in the  $(Q_{G_1}, Q_{G_2})$  plane for the different charge states  $(Q_1, Q_2)$ , where  $Q_{G_i} = C_{G_i}V_{G_i}$ , ( $i = 1, 2$ ). The Coulomb energy  $E_{\text{el}}$  is given by

$$E_{\text{el}} = \frac{1}{3C} \left[ (Q_1 - Q_{G_1})^2 + (Q_2 - Q_{G_2})^2 + (Q_1 - Q_{G_1})(Q_2 - Q_{G_2}) \right]. \quad (19)$$

If two harmonic signals, shifted in phase by  $\pi/2$ , are applied to the gates the system will follow a circular path in the  $(Q_{G_1}, Q_{G_2})$  plane. The type of pump operation described

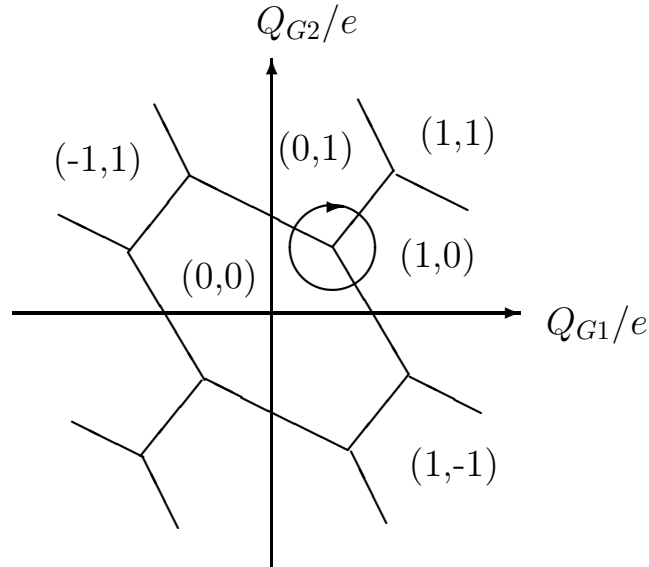


Figure 4: Configuration space for the simplest electron pump operating with two gates. A single electron transfer through the device is obtained when the gate charges follow the circle one turn.

above corresponds to the situation where the circle encloses one of the triple points (*viz.* the transfer between the states  $(0,0)$ ,  $(1,0)$ , and  $(0,1)$ , as shown in Fig. 4). The path in the  $(Q_{G1}, Q_{G2})$  plane can be chosen in many ways and the optimum choice will be discussed in section Sec. 4.3.

### 1.6.2 The turnstile

The simplest electron turnstile contains three islands and four tunnel junctions (upper part of Fig. 5). The turnstile differs from the electron pump by the fact that the external drive frequency needs to be applied only to one gate electrode coupled to the middle island. On the other hand, a non-zero bias voltage is required to define the direction of the current. A single drive signal is an advantage compared to the more complex pump operation. The finite bias is a disadvantage since it causes energy dissipation in the device. At the very low temperatures, required for the proper operation of SET devices, this can be a major problem since the transfer of heat from the metal islands to the substrate is poor which causes heating of the electron gas. This makes the turnstile less favourable for high precision usage.

The operation of the turnstile is illustrated in the lower part of Fig. 5, which displays regions of minimum Coulomb energy in the  $(V_G, V)$  plane for different numbers  $N$  of additional electrons on the middle island. For a finite value of the bias voltage  $V = (V_L - V_R)$  and  $V_G = 0$ , the turnstile is in the  $N = 0$  region. The turnstile cycle starts by increasing the potential of the gate electrode. When the system leaves the  $N = 0$  region, an electron tunnels from the left electrode, via the two junctions on the left, onto the middle island. This brings the system to the  $N = 1$  state. By subsequently lowering the gate potential, the system returns to the  $N = 0$  state as an electron tunnels from the middle electrode, via the two junctions on the right, to the right electrode. In this way a single electron charge is guided through the turnstile for every cycle of the gate voltage.

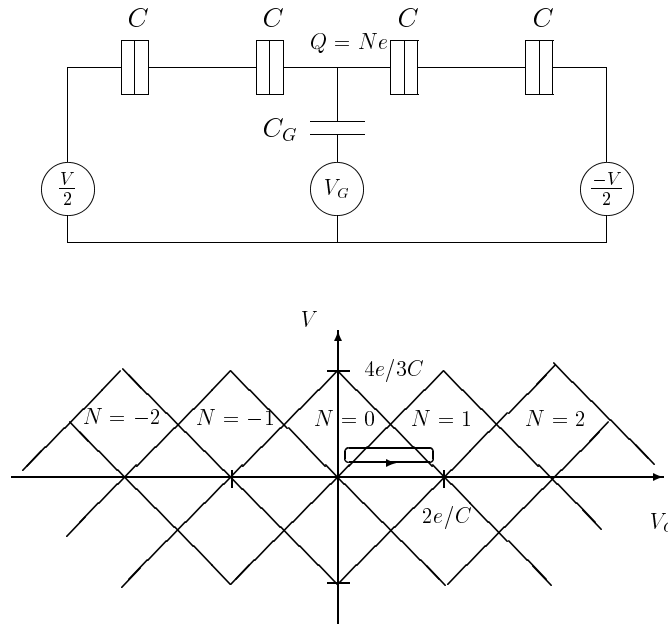


Figure 5: Schematic layout of the single-electron turnstile device. The device has four small tunnel junctions and a gate capacitance. In the lower part of the figure, the stability diagram in the  $(V_G, V)$  plane is shown. Each square represents a stable configuration with  $N$  electrons on the middle island. The ratio of the tunnel junction capacitance and the gate capacitance has the optimum value:  $C/C_G = 2$ . One turn around the operation trajectory depicted in the lower part, transfers one electron through the device in the direction given by the bias voltage.

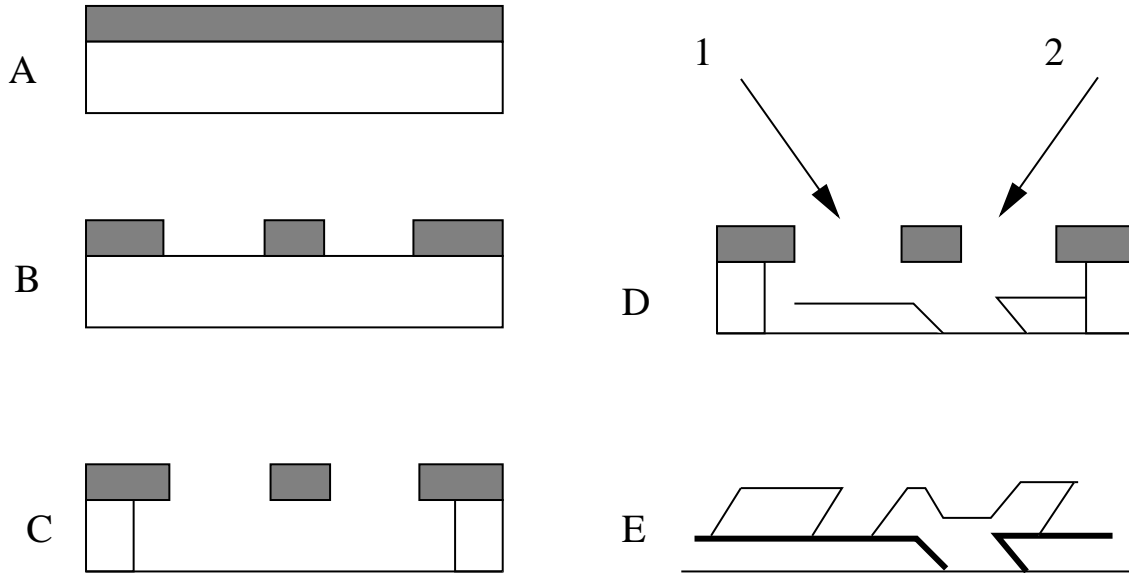


Figure 6: Illustration of the double angle evaporation technique. Starting with a substrate covered with resist (A), a pattern is written using electron beam lithography. After development (B), the structure is etched in several steps, such that a free-hanging bridge is created (C). A metal layer is then evaporated (D) from angle 1, and after oxidation and evaporation of the second metal layer from angle 2, the material used to form the mask is removed and the tunnel junction is created (E). Note that due to the double angle evaporation two copies of each feature are produced, as can be seen in Fig. 7.

## 2 Experimental status of pumps and turnstiles

### 2.1 Fabrication technique

In order to actually realise the devices that were discussed in Secs. 1.5 and 1.6, the conditions set in Eqs. (8) and (9) must be met experimentally. The smallest structures, with known geometry and well controlled tunneling resistances, that can be fabricated using nanoscale technology yield capacitances of the order of parts of a femtofarad. This means that the operating temperatures must be significantly lower than 1 K, which can be obtained by the use of a dilution refrigerator.

The commonly used fabrication technique for SET devices is the so-called double angle evaporation technique. A resist layer is applied onto some substrate. Using electron beam lithography a pattern is written in the resist layer. After development of the resist the resulting nanometer pattern is used as a mask for the evaporation of (usually) Al. The evaporation is performed under two angles with an intermediate oxidation step. The tunnel barriers are formed by the oxidization of the first aluminum layer. The technique is clarified in Fig. 6. Nowadays, tunnel junctions with typical dimensions of  $50 \times 50 \text{ nm}^2$  can be made more or less routinely. Using this technique, different types of metals can be applied to make a variety of junction types: normal-insulating-normal junctions (NIN, e.g., Al/Al oxide/Al junctions exposed to a small magnetic field), superconducting-insulating-superconducting junctions (SIS) and superconducting-normal-superconducting junctions (SNS). Transport through the latter two types of junctions takes place by means of Cooper pairs.

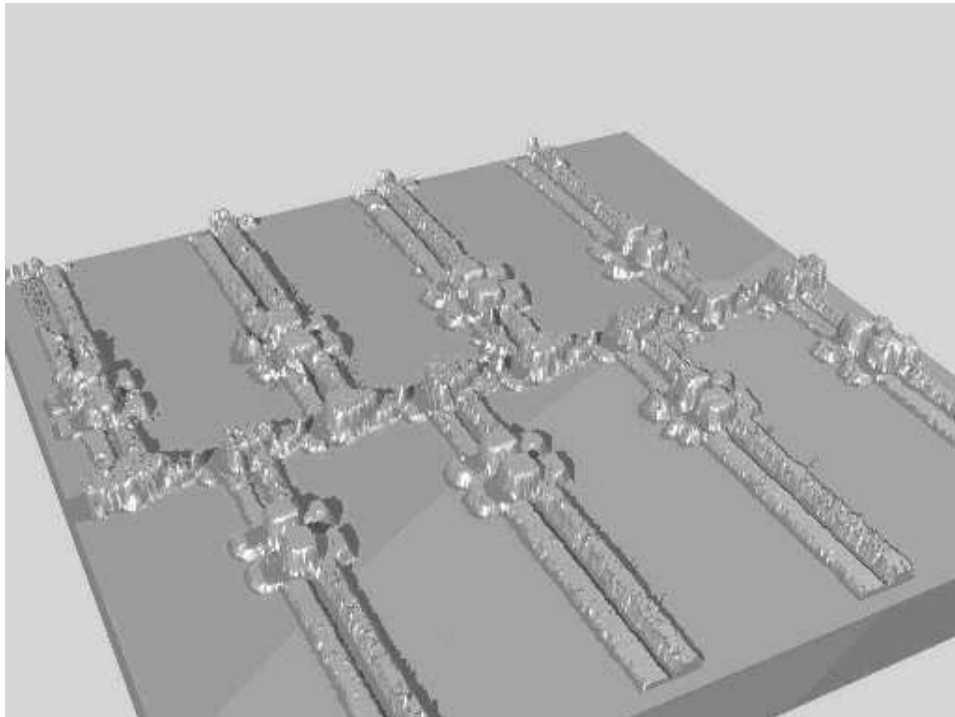


Figure 7: Atomic force microscope image of a part of a seven junction single-electron pump [18]. The shadow evaporation explained in Fig. 6, results in a structure where each feature appears twice (e.g. the two parallel leads leading to the capacitances). The size of the island is approximately  $700 \mu\text{m}$ , and the height of each layer is approximately  $50 \text{ nm}$

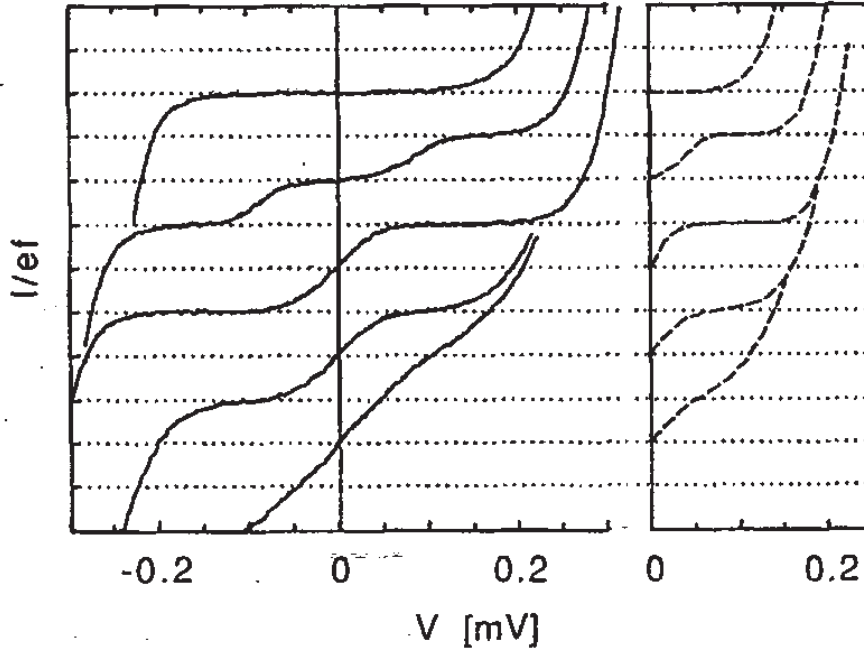


Figure 8: Current-voltage characteristics for turnstiles by Geerligs *et al.* taken from Ref. [13]. The left panel shows experimental data. The right panel is a comparison with numerical solutions of the master-equation. The lower curve is without applied ac potential on the gate and the next ones are for increasing ac power. Dotted lines indicate the expected plateau value,  $I = ef$  for the 5 MHz applied signal.

## 2.2 Uncertainty

In the early 90's the first turnstiles were made at Delft University of Technology [13, 46, 47] and the first electron pumps were fabricated at the Centre d'Etudes Nucléaires de Saclay [14, 48].

Measurements on a four-junction turnstile [13] is shown in the left part of Fig. 8. In the right part of the figure, calculated  $I - V$  curves are plotted. The calculations are based only on classical tunneling probabilities (see Eq. (14)), not taking into account cotunneling (see Sec. 3). The value of the generated current when operating at the plateau agreed with  $I = ef$  within the measurement uncertainty of 0.3 %. Despite the first promising results, no determination of the turnstile current with a higher accuracy has been reported since 1990, even though the group in Delft University of Technology later continued the work on turnstiles [49] using more advanced fabrication techniques.

In 1994 a 5-junction electron pump was fabricated at NIST with an accuracy, expressed in terms of the error per pumped electron, of 0.5 part in  $10^6$  [15]. The equivalent diagram of this pump is shown in Fig. 9(a). The sequence of triangular-shaped voltage pulses, optimized according to Ref. [50], was applied to the four gate electrodes, shown in Fig. 9(b). The pulses were carefully designed to compensate for cross-capacitances. The electron pump was used to transfer an electron to and from the neighboring island, so that the average charge transport in time is zero. The charge on the island was monitored by

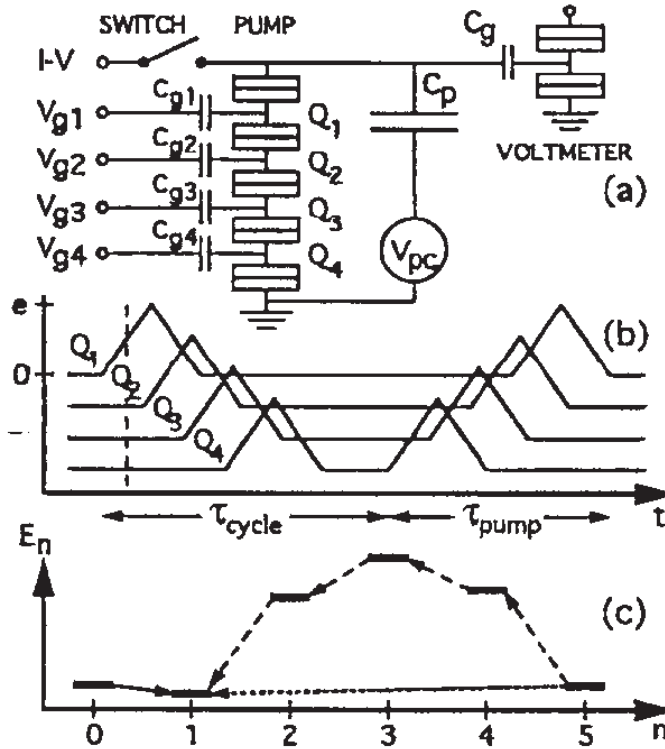


Figure 9: Electrical diagram and operational principle of a 5-junction pump, taken from Ref. [15]; (a) shows the equivalence diagram, (b) the sequence of charge polarizations applied to the islands (the traces are offset for clarity), (c) the Coulomb energy  $E_n$  versus an electron on island  $n$  at time indicated by dashed line in (b). The solid arrow is the desired tunneling, while dashed and dotted arrows show unwanted thermal or cotunneling processes, respectively.

a SET transistor, which was capacitively coupled to the island. In this way the error rate of the pump was determined.

The next generation of pumps made at NIST contained 7 junctions [16, 17, 18]. In Fig. 7 an atomic force microscope picture of such a pump is shown. For this type of pump the error per pumped electron was reduced to 1 part in  $10^8$ . This intrinsic error rate is already low enough to try to realize a capacitance standard as discussed in Sec. 1.3.

### 3 Error mechanisms

There are a number of error mechanisms which deteriorate the high-accuracy operation of single-electron devices. Some of these errors are due to classical effects (cycle missing and thermally activated tunneling), whereas others are due to the quantum mechanical nature of the electron transport (co-tunneling and photon assisted tunneling), which becomes increasingly important at low temperatures. In the next subsections we explain the physics of these error events. We will not review the calculation of the combined error rates. For those results, we refer to the original articles, e.g. the table in Ref. [50] and the numerical works reviewed in Sec. 4.

### 3.1 Cycle missing

When a single electron device is driven by signals of sufficiently low frequency, the distribution of electrons on the islands will at any time correspond to the state with the lowest energy. This is called the *adiabatic* regime. At higher frequencies the electrons are not given enough time to tunnel to the state with lower energy and the device operates *non-adiabatically*. In other words, in this regime a so-called cycle missing may occur. For example, in the electron pump a tunneling event may be missed when we circulate around the triple points as shown in Fig. 4 and the boundaries between the different charge states are crossed too rapidly. This means that on the average less than one electron is transferred per cycle, which leads to deviation from the ideal behaviour as described by Eq. (1).

The analysis of a 3-junction electron pump with harmonic drive has been carried out in Refs. [51, 52]. It was found that reliable operation is only possible for frequencies much smaller than  $1/(R_T C)$ , where  $C$  is the junction capacitance. For an  $N$ -junction pump, the error can be estimated by calculating the probability that an electron does not tunnel during the time where one of the gate charges, say  $Q_1$ , raises from 0 to  $e$ . This results in a error rate per cycle of [50]

$$\varepsilon = \exp\left(-\frac{N-1}{8N^2 R_T C f}\right), \quad (20)$$

where  $f$  is the operation frequency. From these expression it is clear that it is the  $R_T C$ -time that sets the limit for the operation speed. A small  $R_T C$  time is desirable for high speed performance, but, on the other hand, a small tunnel resistance  $R_T$  will lead to large quantum fluctuations and unwanted tunneling events such as cotunneling, described in Sec. 3.3.

In order to minimize the cycle missing error it is important to optimize the waveform of the applied signals. In this way the time spent in a state where the expected tunneling is energetically favorable, can be maximized. For the turnstile a square-type wave form rather than a sinusoidal wave form is preferable. For the pump a triangular signal with optimized amplitudes is used in metrological experiments [15, 16, 17, 18]. Further optimization of the waveform using numerical algorithms is reviewed in Sec. 4.3.

### 3.2 Thermally activated errors

Thermally activated tunneling is the main source of errors at high temperatures. In Fig. 9, a series of thermally enhanced tunneling events is indicated by the dashed arrow. From Eq. (14) it follows that the tunneling rate is suppressed exponentially if the energy of the final state is much larger than the energy of the initial state,

$$\Gamma_{\text{thermal}} \approx \frac{|\Delta^\pm|}{e^2 R_T} \exp(-|\Delta^\pm|/k_B T). \quad (21)$$

One can thus calculate the probability of a sequence of tunneling the events. By taking into account the most important sequences, Jensen and Martinis [50] found approximate formulas for the error rate per cycle due to thermally activated processes

$$\varepsilon_{\text{thermal}} \approx c \exp\left(-d \frac{E_c}{k_B T}\right), \quad (22)$$

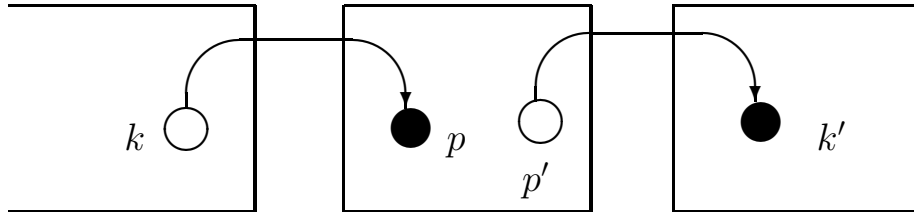


Figure 10: Cotunneling event in a SET transistor. Two electrons tunnel in a coherent way such that the charge on the island is the same in the initial and the final states. Therefore the process overcomes the Coulomb energy barrier, but is suppressed due to limited number of available final states in phase space. Furthermore, the probability of the two electron process is proportional to the product of the two tunneling conductances.

where the parameters  $c$  and  $d$  depend on the number of junctions and the bias voltage. This expression was confirmed by numerical simulations. For the parameters of the accurate pump described in Sec. 2.2, the thermal errors dominate for temperatures larger than 100 mK, but are strongly suppressed for lower temperatures.

If the system does not have to relax between tunnel events the electron gas heats up and consequently the electron temperature is higher than the lattice temperature. The elevated temperature is a result of a balance between input power and the relaxation due to electron-phonon coupling[37, 36]. The cooling power is decreasing at low temperatures as a power law approximately as  $\Sigma VT^5$ , where  $V$  is the volume and  $\Sigma$  is a dissipation constant. On the other hand, the input power is proportional to the driving frequency and the charging energy,  $fE_C$ . Using this line of reasoning an estimated electron temperature of 80 mK was found in Ref. [37] using typical parameter for metallic single electron pump devices,  $f = 10$  MHz and a base temperature of 10 mK. From this consideration it is evident that there is a limit to the lowest operation temperature for single electron devices.

The understanding of the thermal errors due to tunneling is on firm ground. However, thermal effects may also be important for processes which involve higher order tunneling processes such as thermally activated cotunneling. This is explained in the next section.

### 3.3 Cotunneling

In the master-equation described in Sec. 1.6, we have so far included only the processes where the electron tunneling through a single junction is involved. However, higher order processes are also possible [55]. One such process is a cotunneling event where two or more electrons tunnel simultaneously through several junctions in a quantum-coherent manner.

In the case of the SET transistor, explained in Sec. 1.5 a two electron cotunneling process can transfer an electronic charge from left lead to the right lead such that the number of electrons on the island is the same in the initial and the final state. This process is illustrated in Fig. 10. There are two possible intermediate states, one where an electron jumps through the right barrier first leaving an excess hole on the island and one where an electron jumps through the left barrier first.

There are two fundamentally different types of cotunneling processes: if the state of the electron that enters the island is identical to the state of the electron that leaves the island the process is called an *elastic* cotunneling process whereas if the two states are different it is an *inelastic* process. The latter is generally dominant for the metallic systems where the island has a large number of electronic states [56].

In Section 1.5 we derived the tunneling rate using Fermi's golden rule. The cotunneling rates can be derived in a similar fashion except that now we must include processes of higher order in the tunneling matrix elements which connect electronic states across the tunnel junctions. The effective matrix elements for the inelastic cotunneling process depicted in Fig. 10 can be found using quantum mechanical perturbation theory. Since it is a quantum mechanical process energy need not be conserved in the intermediate state, i.e., the state immediately after the first electron has tunneled. Furthermore, the different possible intermediate states add *coherently* and the effective matrix element  $\hat{T}$  (which should be entered in golden rule formula (13)) between initial and final state becomes

$$\langle f|\hat{T}|i\rangle \approx \frac{1}{\epsilon_k - \epsilon_p - E^+} + \frac{1}{\epsilon_{p'} - \epsilon_{k'} - E^-}. \quad (23)$$

The electrostatic energy differences between the initial and the two possible intermediate states denoted by  $E^+$  and  $E^-$  correspond to adding or removing an electron from the island, respectively. In order to find the rate for transfer of an electronic charge from left to right one must sum over all  $k, k', p, p'$ , and furthermore include appropriate occupation probabilities. At zero temperature these integrals can be performed [55].

At low temperature and small bias  $k_B T, eV \ll E^\pm$  one can approximate the intermediate state energies in denominators in Eq. 23 by the electrostatic energy differences, because energy of the electron-hole pairs is limited by temperature and bias voltage. In this case one finds for the cotunneling rate through the device from left to right [56]

$$\Gamma_{\text{cotun}}(L \rightarrow R) \approx \frac{G_L G_R \hbar}{12\pi e^3} \left( \frac{1}{E^+} + \frac{1}{E^-} \right)^2 \left[ (2\pi k_B T)^2 + (eV)^2 \right] \frac{V}{1 - \exp(-eV/k_B T)}, \quad (24)$$

where  $V$  is voltage drop across the device.

The approximate formulae Eq. (24) and the zero temperature result has been tested in several experiments [57, 58, 59, 60] and very good agreement was found. However, outside the range of validity for the approximations, i.e. in the cross-over between the cotunneling dominated and sequential tunneling dominated regimes the theory [55, 56] gives unphysical divergences in the cotunneling rate and needs to be modified.

To repair the possible divergence in (23) several authors [58, 61, 62, 63, 64] have included a life time broadening due to tunneling in and out of the island. The life time broadening results in a imaginary term in the denominators of Eq. (23) and in this way a gradual cross-over between the cotunneling and the sequential tunneling limits is obtained. Comparison with experimental data has shown that good agreement is obtained for not too small tunnel resistances [58, 65]. In passing we note that recent work by König, Schoeller and Schön [66] has shown that a thorough second order perturbation theory, which does not suffer the divergence problem, gives very good agreement with experiment even for rather small tunnel resistances [67]. Unfortunately, these approaches are complicated and it is not clear at this point whether generalization to the cotunneling through many junctions can be made sufficiently effectively for practical numerical analysis of multi-junction devices. In order to have a simple way of evaluating the cotunneling contributions, Jensen and Martinis [50] have proposed the following approximation scheme. They evaluated the integration over intermediate states by distributing energy difference between initial and final states equally among the electron-hole pairs. This means that for the matrix element in Eq. (23),  $\epsilon_k - \epsilon_p = \epsilon_{p'} - \epsilon_{k'} = (E_i - E_f)/2$ . Fonseca et al. improved this approximation by shifting the lowest order tunneling rate in Eq. (14), to lower energies. By doing this these authors obtained a smaller difference between the

approximate tunneling rate and the one obtained from the more correct higher order approximations citepasq93,koro92,naza93b,aver94,flen97,lafa93.

The expression for several consecutive cotunneling events was derived by Averin and Odintsov [55]. The Jensen and Martinis and the Fonseca et al. approximations are easily generalized for the multiple cotunneling case and they are used in the numerical simulations of pumps and turnstiles, reviewed in Sec. 4. We give here the final expression for the multiple cotunneling events of order  $n$  [50], because it is the dominant source of error at the lowest temperatures:

$$\Gamma_{\text{cotun}}^{(n)} = \frac{2\pi}{\hbar} \left( \prod_{i=1}^n \frac{\hbar G_i}{2\pi e^2} \right) S^2 F_n(\Delta E_n), \quad (25)$$

where  $G_i$  is the conductance of tunnel junction number  $i$ ,  $\Delta E$  is the energy difference between final and initial states, and

$$S = \sum_{\text{permutations}} \left( \prod_{k=1}^{n-1} \frac{1}{\Delta E_k - \Delta E/n} \right) \quad (26)$$

where the sum is over all permutations of cotunneling sequences going from initial to final state, and finally

$$F_n(\Delta E) = \frac{\prod_{i=1}^{n-1} [(2\pi k_B T i)^2 + (\Delta E)^2]}{(2N-1)!} \frac{\Delta E}{\exp(\Delta/k_B T) - 1}. \quad (27)$$

From this expression we see that the higher order cotunneling events are suppressed by the ratio of the junction conductances to the quantum conductance  $e^2/h$  to the power  $n$ . For typical junctions with resistances in the 100 k $\Omega$  range the  $n$  order cotunneling process contains a factor  $(0.04)^n$  due to the first product of Eq. (25). However, in contrast to the thermally activated tunneling it is not exponentially suppressed and the cotunneling leakage events will thus dominate at low temperatures.

One way of suppressing cotunneling is to increase the number of Coulomb islands. Another method which was suggested in Ref. [69] is to increase the resistance of the leads that couples to the device. The authors of ref. [69] showed that for a two junction circuit the cotunneling rate the cubic voltage dependence in Eq. (24) is replaced by  $\Gamma_{\text{cotun}} \sim V^{3+2z}$ , where  $z = Re^2/h$  is the normalized resistance of the leads. This idea is now being pursued experimentally[70]

Finally, we mention the so-called *elastic* cotunneling, which means that energy is not dissipated to electron hole pairs in the tunneling process. Consequently, the electron states  $p$  and  $p'$  in Fig. 10 are the same. In other words, it is “the same electron” that enters and leaves the island. The probability of elastic cotunneling is proportional to the single particle level spacing [56]. Thus the process is generally very weak for metal islands. However for semiconductor devices this effect indeed gives significant contributions to the electron transport.

### 3.4 Photon assisted tunneling

When a SET device is irradiated by an external electromagnetic field, the potentials on the electrodes will oscillate. Tunneling events which are otherwise not possible may now occur through absorption of photons from the external source. Only small amounts of

electromagnetic radiation are needed to introduce considerable errors due to photon assisted tunneling [71]. Therefore careful attenuation of the high frequency noise is necessary by means of shielding, thermally anchoring all leads in the cryostat, and applying copper powder filters [72], lithographically made miniature filter [73] or lossy coaxial cables [74].

When the device is driven by a periodic signal as in the pump or turnstile, it is possible that the drive itself induces photon assisted cotunneling events. This effect was considered in Ref. [64], but it was found that only at a frequency higher than several gigahertz this error contribution becomes significant. It can thus be neglected for present days pumps and turnstiles operating at typically 5-10 MHz.

### 3.5 Background charges

Noise introduced by a random motion of charges in the dielectric surrounding (the substrate, the barriers of the tunnel junctions, etc.) of the conducting islands is a serious problem in SET devices. This noise leads to fluctuations of the island's polarization. Usually, the frequency dependence of the noise spectral density is close to  $1/f$ , although sometimes it exhibits an almost  $1/f^2$  dependence in combination with a telegraph-like time dependence [49, 75]. This switching noise results from one or several two-level fluctuators with typical switching times ranging a fraction of a second up to minutes. For most of the aluminium-based SET devices, fabricated on various substrates ( $\text{SiO}_2$ , Si,  $\text{Al}_2\text{O}_3$ ) the intensity of the background charge noise at 10 Hz is between  $10^{-4}$  and  $10^{-3} e/\sqrt{\text{Hz}}$  [49, 75, 76, 77].

However, in the devices fabricated with a stacked design the islands are partly [78, 79, 80] or entirely [79, 80] screened from the substrate by an underneath gate or by an underneath counter electrode. Such devices exhibit considerably less noise, down to the lowest value measured so far,  $2.5 \times 10^{-5} e/\sqrt{\text{Hz}}$  at 10 Hz [79, 80]. The dominating role of substrate in causing the background charge noise is also proven by the mutual correlation observed in the cross spectrum of the  $1/f$  noise of two SET electrometers which were closely positioned on the same substrate [77, 81]. Therefore, a suitably chosen substrate and/or an appropriate geometry for SET devices should reduce the background charge noise.

The effect of background charges, as discussed above, is not limited to time dependent fluctuations. The dc offset charges [15, 17] can also arise due to charges trapped inside the substrate and the barriers of the tunnel junctions, and due to different work functions of dissimilar electrode materials [82].

## 4 Numerical analysis of single electron devices

### 4.1 Methods and tools for numerical analysis

Analytical treatment of the single-electron transport is only possible for circuits with few tunnel junctions such as the SET transistor, or symmetric devices such as one-dimensional tunnel junction arrays. In the last few years, several computer codes have been developed to analyze complex single electron circuits numerically [83, 84, 85, 53, 54, 86]. Two main approaches have been used. Firstly, Monte Carlo algorithms [87, 88, 89, 84, 86], which average over various realizations of stochastic SET events. Secondly, algorithms based on a numerical solution of the master equation (18), which describes the dynamics of SET

circuit in terms of time-dependent probabilities of various charge configurations [50, 51, 53, 54, 85, 86, 90].

The advantage of Monte Carlo routines is their relative simplicity and robustness. This makes them convenient tools for the study of the dynamics of single electron systems, for which rare events are not important. Another feature of the Monte Carlo method is the trade-off between accuracy and simulation time: one can quickly achieve approximate results for very large circuits, which otherwise would not be possible to compute. An intrinsic drawback of Monte Carlo algorithms is their inefficiency in the analysis of rare events, simply because these rare events might not be encountered during the simulation time. Specifically we mention the codes MOSES [84] and SIMON [86] which are able to analyze arbitrary circuits consisting of tunnel junctions, capacitances, resistors, and signal sources. The latter code is convenient because of its graphical user interface.

Reliable simulations of SET devices require realistic estimates of the contributions of rare events. This can be achieved by starting from the master equation (18), whose solution contains *complete* statistical information about the dynamics of the system including the probabilities of the rare events. The problem with the master equation method is the necessity to trace the time-evolution of a large number (up to several thousands) of charge states. This makes the computation time-consuming. The analysis is alleviated in the case of adiabatic devices (like single electron pump) where the electron transfer occurs at low energies compared to  $E_C$  and the master equation involves a moderate number of low energy charge states [50, 51, 90]. In order to use the master equation approach for general, non-adiabatic devices (like turnstiles) the development of more sophisticated algorithms is required. In the following section, we will briefly describe an effective algorithm of this type that is based on the ideas of global analysis and the dynamical choice of the basis of states [85, 53, 54].

Finally, we mention the attempt to combine the Monte Carlo approach with solution of the master equation [86]. An essential assumption of this method is that the system can stay in a rare state for a period much shorter than the characteristic time of the simulation (e.g. the period of an external signal in case of pumps). This assumption in fact means that the errors due to rare events are analyzed *locally* in time. In the following section it is shown that in order to detect errors in the operation of SET devices, the errors should be analyzed *globally*, throughout the whole cycle of the device operation.

## 4.2 SENECA: a global approach to rare events

In this section, we introduce SENECA (Single Electron NanoElectronic Circuit Analyzer), a computer algorithm suitable for studies of the dynamics and statistics of single electron systems consisting of arbitrary combinations of small tunnel junctions, capacitances, resistors and voltage sources [85, 53, 54]. The method is based on the numerical solution of a linear matrix equation for the vector of probabilities of various electric charge states of the system, with iterative refining of the operational set of states. The method is able to describe very small deviations from the classical behavior of a system, caused by the physical error mechanisms discussed in Sec. 3. Below, the main underlying ideas and characteristics of the algorithm are briefly discussed.

*Global analysis of errors.* It must be emphasized that one should distinguish between a rare tunneling event and the error in operation of a device (i.e. deviations from Eq. (1)). Some rare tunneling events bring the system to an unwanted charge state, which afterwards evolves classically to a correct operational cycle. These rare events do not

affect the proper operation of the device. In order to separate those events from the error introducing events, one should analyze the operation globally by solving the master equation throughout the whole cycle.

*Clustering of the charge states according to their probability - iterative approach.* For single electron devices of interest the number  $M$  of islands ranges from 5 to 30. If we consider the charge configurations of the islands with additional charges 0 and  $\pm e$ , the number of states can be roughly estimated as  $3^M$ . Nevertheless, when the temperature is low and the tunnel conductances of the junctions are small, most of the possible transitions (either those leading to an increase in the electrostatic energy, or those of high cotunneling order) have very low rates. As a consequence, a large number of charge states have very low probabilities  $P$  and may be ignored. Hence, an iterative approach is chosen which considers for each iteration  $n$  only the limited number of states for which  $P > P(n)$ . The threshold  $P(n)$  decreases rapidly with  $n$ .

*Dynamical choice of the basis of states.* Each iteration corresponds to the solution of the master equation at the time interval of the operation cycle. This interval is divided into enough time steps, so that the variation of external parameters between steps can be neglected. At each time step the algorithm first guesses the set of states whose probabilities are expected to be large enough,  $P > P(n)$ , then solves the master equation for this set, and finally filters out the states whose probabilities at the end of the step turned out to be low,  $P < P(n)$ . In this way the minimum possible basis of states is kept throughout the computation.

### 4.3 Results of simulations

*Pump.* First we consider an  $N$ -junction pump driven by triangular voltage pulses with amplitude  $ae/C_{Gi}$  and offset  $ue/C_{Gi}$  applied to the gates as shown in Fig. 11(a). The gate capacitances are assumed to be small:  $C_{Gi} \ll C$ . If the pump works properly, an electron tunnels sequentially through all junctions of the array following the propagation of the pulse. The region of correct classical operation (disregarding any rare processes) can be evaluated from the condition that tunneling of an electron occurs only in an "active" junction biased by a voltage pulse, while the other junctions are closed. By choosing  $u$  equal to  $(1-a)/N$  one maximizes the region of correct classical operation (Fig. 11(b),

$$|v| < \frac{(N-1)(N-2)}{2N} \min[a, (2-a)], \quad (28)$$

with  $v$  being the bias voltage in units of  $e/C$ .

The closer the parameters  $a$  and  $v$  are chosen to the center of the region (28), the smaller the error due to rare events. In particular, the order  $n$  of cotunneling processes, which, according to Eq. (25) primarily determines the intensity of cotunneling, increases from 2 near the inner borders of this region to  $N-1$  in its central part (dashed area in Fig. 11),

$$|v| < \frac{(N-1)}{2N} \min[a, (2-a)], \quad (29)$$

in which the best performance of the device occurs. In the region (29) the deviation  $\Delta I = I - ef$  of the current  $I$  from its ideal value  $ef$  is determined by two competing cotunneling processes, shown Fig. 9. In one process instead of regular tunneling through an active junction (corresponding, for example, to the transition  $(0,0) \rightarrow (0,1)$  in Fig. 4), the cotunneling occurs through all the other  $N-1$  junctions in the opposite direction

$((0, 0) \rightarrow (1, 0) \rightarrow (0, 1), (1, 0)$  being the intermediate state, see Sec. 3.3). In this process the electron charge is transferred through the device in the direction opposite to the current. The competing cotunneling process starts *after* the regular tunneling event and transfers an electron charge in the direction of the current  $((0, 1) \rightarrow (1, 0) \rightarrow (0, 0)$  in Fig. 4).

In the region of optimal operation (29) the error  $\Delta I$  in the current can be evaluated analytically [50, 90]. The performance of the device can be characterized by the slope of the current plateae,  $G = d(\Delta I)/dV$  at  $V = 0$ . Being multiplied with the size  $e/C$  of the optimal region (29) this gives characteristic scale of the current deviation  $\Delta I^*$ , or accuracy of the device,  $\varepsilon = \Delta I^*/ef = G/fC$ .

We consider first the case of a slow drive,  $k_B T \gg eV_0 \equiv e^2[(N-1)\dot{q}_i R_T/NC]^{1/2}$ ,  $\dot{q}_i \simeq Nf$ ,  $R_T$  being the tunnel resistance of the junctions. In this adiabatic regime the probabilities to find an electron on the left and right electrodes of an active junction correspond to equilibrium conditions at any time. The deviation  $|\Delta I|$  of the current due to cotunneling increases with temperature and does not depend on driving frequency. The accuracy is given by [90, 50],

$$\varepsilon \simeq \frac{Ne^2 R_T}{\hbar C V_0^2} \left( \frac{\pi \hbar}{2e^2 R_T} \right)^{N-1} S^2 (k_B T)^{2N-3}, \quad (30)$$

where the factor  $S$  (given by Eq. 26 with  $\Delta E = 0$ ), can be found explicitly in the center ( $a = 1, u = 0$ ) of the optimal region (29),

$$S = \left( \frac{2NC}{e^2} \right)^{N-2} \frac{N-1}{(N-2)!}. \quad (31)$$

In the opposite case,  $k_B T \ll eV_0$  the tunneling through an active junction occurs non-adiabatically (effectively only a single tunneling event occurs during the gate voltage pulse); the deviation  $|\Delta I|$  of the current due to cotunneling increases with increasing driving frequency and does not depend on temperature [90, 52]. The accuracy can be evaluated as [90, 50],

$$\varepsilon \simeq \frac{e}{CV_0} \frac{NS^2}{(2N-3)!} \left( \frac{\hbar V_0^2}{\pi R_T} \right)^{N-2}. \quad (32)$$

Hence, for a given temperature, the optimal driving frequency corresponds to the crossover point, where the characteristic energy  $eV_0$  of electron tunneling is equal to the energy  $k_B T$  of thermal fluctuations.

So far we have not considered the rare events due to thermally activated classical tunneling whose probability decreases exponentially with temperature,  $P_{th} \sim \exp(-\Delta E/k_B T)$ ,  $\Delta E \simeq E_C$ . The analysis [50] has shown that thermal activation of classical tunneling can be neglected compared to the cotunneling at temperature of the order of or smaller than  $0.025E_C$ , which is usually the case in experiments.

The early estimates [50, 90] of the abovementioned factors confirmed by more recent simulations using SENECA (see Fig. 12) [53, 54] predict that already the 5-junction pump with typical experimental parameters,  $R_T = 300 \text{ k}\Omega$ ,  $C = 0.1 \text{ fF}$ ,  $f = 10 \text{ MHz}$ ,  $T = 100 \text{ mK}$  should have metrological accuracy  $\varepsilon \simeq 2 \cdot 10^{-12}$ . It should be noted that both the cotunneling and thermally activated tunneling can be effectively suppressed further by increasing the number of the junctions and decreasing the junction size (and/or the operation temperature).

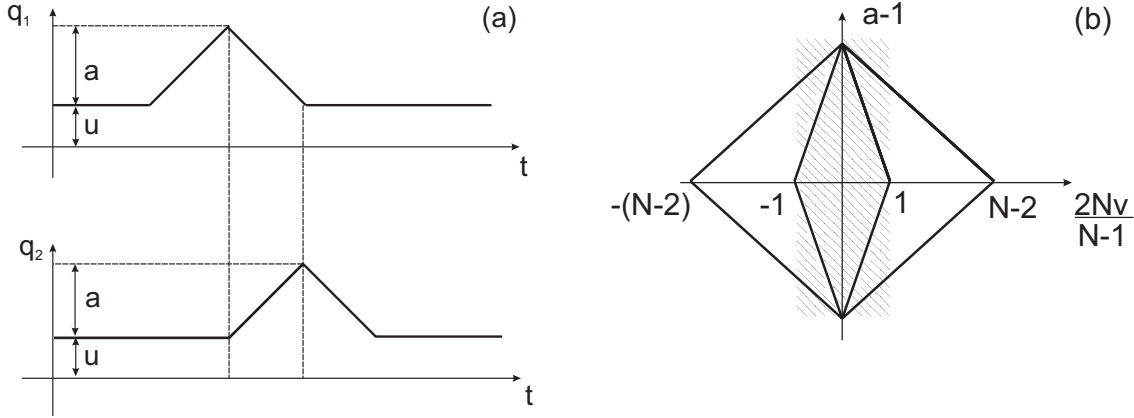


Figure 11: (a) The shape of the modulation of the gate voltages  $V_{Gi}$  ( $q_i = C_{Gi}V_{Gi}/e$ ) in the pump device. (b) The region of correct classical pump operation in  $(a, v)$  plane (see text). The dashed area is the region where the lowest order of allowed co-tunneling transitions is  $N - 1$ . From Ref. [90].

Another way of improvement of the pump operation is the optimization of the driving voltage pulse shape [53, 54]. The idea is based on the consideration of the energy dependences of the classical tunneling, Eq. (14),  $\Gamma_{cl} \propto \Delta E$  and cotunneling rates  $\Gamma_{cot} \propto \Delta E^{2N-1}$ , Eq. (25). To minimize the ratio  $\Gamma_{cot}/\Gamma_{cl}$  one has to decrease  $\Delta E$  during the "active" portion of the time interval when the electron transfer between the islands occurs. When the probability of the transfer is close to unity, one increases  $\Delta E$  to ensure the full transfer of an electron during the "passive" portion of the interval. Being optimized by SENECA algorithm, this two-step drive improves the calculated accuracy of 5-junction pump (Fig. 12) by a factor of 30 for  $k_B T \simeq 100$  mK and other parameters given above (the improvement enhances at lower temperatures).

*Turnstile.* The diagram of correct classical operation of the turnstile with  $2N$  junctions is shown in Fig. 13 (see also Fig. 5). Being driven by the gate voltage alternating between the two dashed regions in Fig. 13 the device transfers one electron per cycle of the gate voltage. The regions are defined by [90]

$$u + v > (1 + c)(N - 1), \quad u - v < (1 + c)(N - 1) \quad (33)$$

$$u + v < (3 + c)N - 1 - c, \quad v - u < (1 + c)(N - 1) \quad (34)$$

and similar pair of equations with  $u \rightarrow -u$ . Here  $u = (2C_g V_g / e - 1)N$ ,  $v = (2C + NC_g)V/e$ ,  $c = NC_g/C$ .

Analysis [90] shows that the order of cotunneling transitions reaches its maximum  $n_0 = 0.8N$  ( $N \gg 1$ ) for  $c < 2/3$  and the voltages near the threshold of correct classical operation ( $u_{high} + v = (1 + c)(N - 1)$ ,  $u_{low} - v = -(1 + c)(N - 1)$ , see Fig. 13). This happens at the optimal voltage  $V_{opt} = (1 + c)(n_0 - 1)e/[2(2 + c)C]$ . Careful numerical optimization [53, 54] of the accuracy of 6 and 8-junction turnstiles as function of the gate capacitance  $c$  and the amplitude  $u_{high} = -u_{low}$  of the gate voltage has shown that the optimal gate capacitance corresponds to  $c \approx 2/3$ . The calculated uncertainty of 8-junction turnstile with optimized parameters was better than 1 part in  $10^9$  for  $R_T = 300$  k $\Omega$ ,  $C = 0.1$  fF,  $f = 10$  MHz, and  $T = 100$  mK (see Fig. 14).

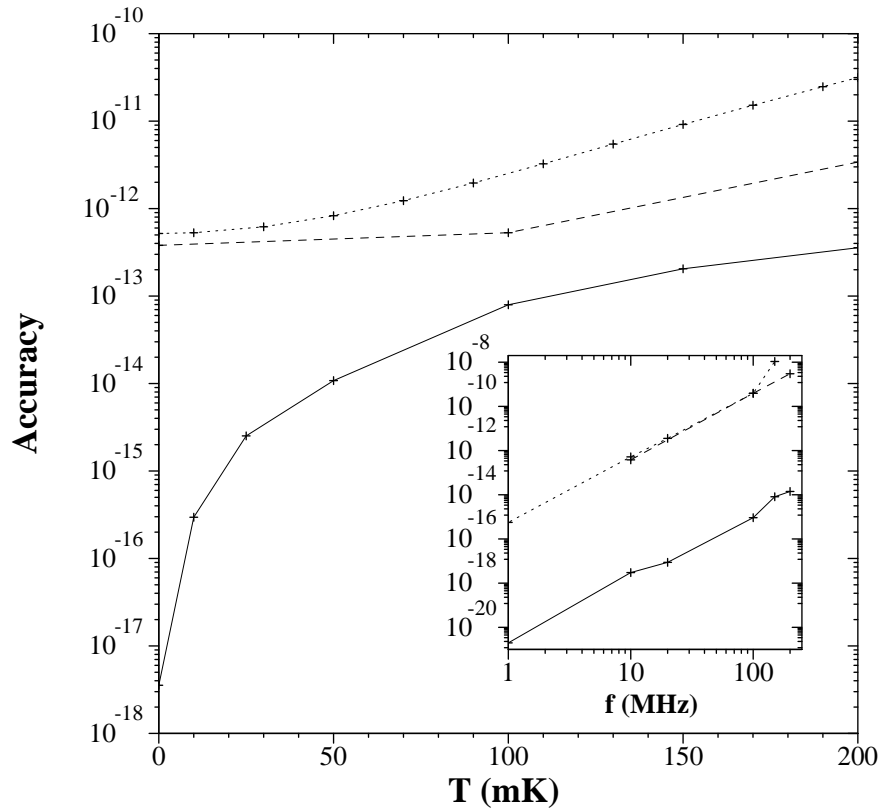


Figure 12: Accuracy of the 5-junction pump driven by optimized step-like waveform (solid line), triangular waveform with optimized tunnel resistances (dashed line), and triangular waveform with fixed tunnel resistances  $R_T = 300 \text{ k}\Omega$  (dotted line). The insert shows the accuracy as a function of driving frequency at  $T = 0$ . From Ref. [53].

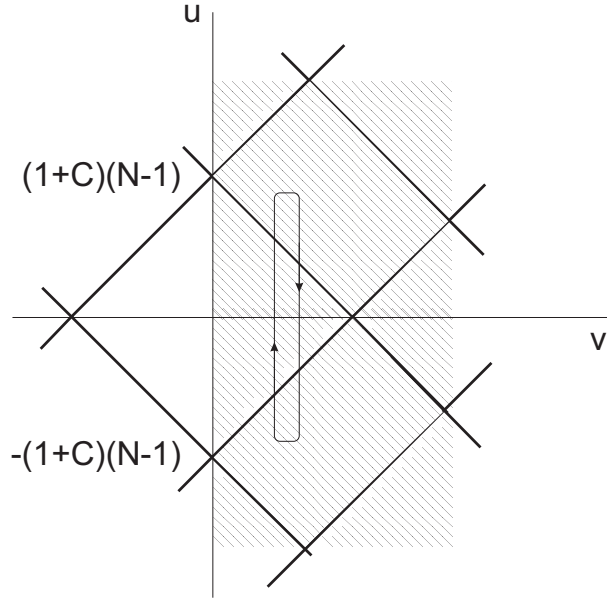


Figure 13: The diagram of the turnstile operation in the  $v-u$  plane,  $v = (2C + NC_G)V/e$ ,  $u = N(2C_G V_G/e - 1)$ . In the upper dashed region an electron is pulled in the turnstile, in the lower dashed region it is pushed out. The central square corresponds to the Coulomb blockade state where all classical transitions are suppressed. From Ref. [90].

*Hybrid pump-turnstile.* In order to reduce the number of parameters (dc gate voltages, amplitudes and phases of RF gate voltages, bias voltage) controlling the operation of a pump device, it has been proposed to apply RF signal to every second gate of the pump. The calculated uncertainty of a properly biased pump-turnstile with 6 junctions [53, 54] was close to the uncertainty of unbiased pump (2 parts in  $10^{12}$  for the parameters listed above), but deteriorated to 5 parts in  $10^9$  for unbiased device, see Fig. 14.

## 5 Comparison of theory and experiments

### 5.1 Discrepancies between measured and predicted errors

The experiments reviewed in the Sec. 2 have demonstrated an error per pumped electron of the order of 1 part in  $10^8$  for pump-like SET devices. Up to very recently, the development followed the most obvious path, namely the improvement of the accuracy by increasing the number of tunnel junctions (which suppresses cotunneling) and the reduction of their size (which enhances the Coulomb blockade). In particular the 7-junction pump has been very well characterized [18] with respect to the capacitances of the individual junctions, the offset charges at the islands, as well as the electron temperature.

Substantial efforts have been made [15, 18] to compare the observed accuracy of the pump device with theoretical predictions and to identify unforeseen error mechanisms. Some details of the experiments are given in Sec. 2.2.

For the 5-junction pump [15] the error per pumped electron at 40 mK has been observed to be exponentially dependent on pump frequency for frequencies higher than 5 MHz. This behaviour is expected when cycle missing is the dominant error mechanism

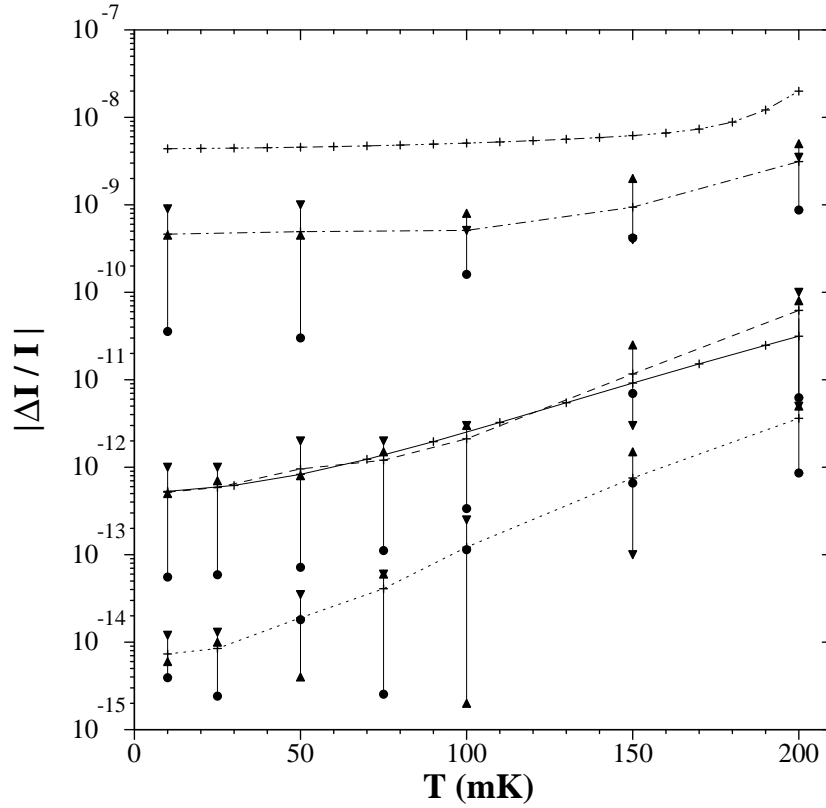


Figure 14: Deviation of the current from the quantized value in the unbiased (solid line) and biased (dotted line) 5-junction pump, unbiased (dot-dot-dashed line) and biased (dashed line) 6-junction hybrid pump (all driven by a triangular waveform), and 8-junction turnstile driven by a step-like waveform (dot-dashed line) at  $f = 10$  MHz as functions of temperature. Circles: current deviation at the inflection point  $V_0$ , triangles up (down): current deviation at  $V_0(1 \pm 0.1)$ . From Ref. [54].

(see 3.1). However, for frequencies smaller than 5 MHz, the observed error per pumped electron at 40 mK saturates at a level of 1 part in  $10^6$ . This saturation, when ascribed to thermally activated processes and cotunneling, occurs at a value that is  $10^8$  times larger than expected. In order to explain this very large discrepancy Martinis *et al.* [15] suggested that the excess error is caused by an additional source of energy, e.g. by leakage of thermal noise generated at 4 K or by energy released by charge traps in the substrate.

For the 7-junction pump [16], the measured error per pumped electron at 140 mK, when the dominant error mechanism is thermally activated tunneling, has been found to be 1 part in  $10^6$ . This is in reasonable agreement with the theoretical estimate of 1 part in  $10^7$ . However, at 40 mK, when the dominant error mechanism is cotunneling, the measured error per electron amounts to 1 part in  $10^8$ , which is in sharp contrast to the theoretically predicted value of 1 part in  $10^{20}$ . Since the error per electron is constant and only weakly dependent on the wait time between the transfer of individual electrons, the errors are concluded to occur predominantly during the active pumping cycle. Therefore, the error mechanisms in the pump mode and hold mode are likely to be different.

Despite the fact that this 7-junction pump exhibits a much smaller error per electron than the 5-junction pump, this improvement is not as drastic as expected from theory, especially in the temperature range below 100 mK.

## 5.2 Possible sources of additional error mechanisms

As mentioned in the previous section, additional error sources can exist due to 4 K radiation or trapped charges in the substrate. Usually, in order to prevent 4 K radiation from reaching the device, special microwave filters are placed in series with every electrical lead. In addition, the device is mounted in an electromagnetically shielded box. Surprisingly, it was shown [18] that removal of the filters and the shield does not necessarily affect the error rate of the 7-junction pump. This hints at a strong internal low-temperature source of spurious tunneling events, which is much stronger than the external noise. It is also possible that photons are generated by non-equilibrium charge fluctuations in the substrate and/or the tunnel barriers (see Sec. 3.4 and Ref. [91]). Such an intrinsic photonic source cannot be filtered, and may present a fundamental problem for metrological and digital application of SET devices.

Note that it can be difficult to separate the effect of high frequency photons due to the charge fluctuations from the effect of low frequency noise due to the drift of the offset charges. However, in the experiments reported by Ref. [18] the comparison with theory was made when the optimal background charge compensation was stable. Often the devices were kept at millikelvin temperatures for several weeks, after which movement of background charges was very small and adjustments of the dc voltages on the gate lines was only necessary with time intervals of tens of hours.

## 6 Alternative designs for single-electron current standards

The main disadvantage of the discussed current standards based on normal SET junctions is their relatively low operation frequencies of a few megahertz, which correspond to a current level of only a few picoampere. This limitation is caused by the necessity to have large tunnel resistances for the normal junctions  $R_T \gg R_Q \equiv h/e^2$  in order to fulfill the condition of the charge quantization. The limitation in frequency may however be circumvented in several ways, as will be discussed in this section.

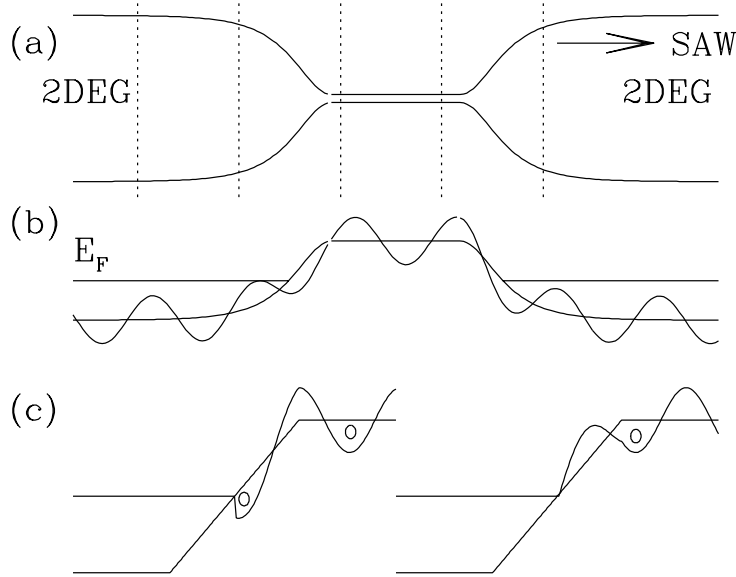


Figure 15: Schematic outline of a SETSAW device. (a) shows the two 2DEGs separated by a narrow constriction. Propagating SAWs are indicated by dashed lines. (b) illustrates the potential landscape along the center of the device. In the constriction region a potential barrier is present. The SAW induces a propagating modulation of the potential. In the 2DEG region the modulated potential induced by the SAW is screened and the resulting potential is shown in (c) for two different times. In the left part of the figure an electron scooped up by a minimum in the potential after which it is moved upward into the constriction region (right part of figure).

### 6.1 Surface acoustic waves as carriers of single electrons

The interaction of surface acoustic waves (SAW's) with a two-dimensional electron gas (2DEG), present at the interface in a GaAs-AlGaAs heterostructure, can be applied to generate an electrical current that is determined by the frequency of the SAW. In Fig. 15 the working principle of the so-called SETSAW device is outlined. Due to the piezoelectric effect the SAW creates a propagating modulation of the electrostatic potential through the 2DEG. Normally this modulation is screened by the electrons in the 2DEG. By using a split-gate technique a quasi-one-dimensional channel is formed in the 2DEG. By applying a sufficiently negative voltage to the split gate the electrostatic potential in the constriction is increased and the electron density can be reduced to zero (pinch-off regime). In this case a propagating modulation in the channel is no longer screened. For a sufficiently strong amplitude of the SAW the quasi-one-dimensional electron gas in the constriction is split into a sequence of small islands, or quantum dots, moving with the velocity of the SAW.

Recently it has been shown that such a technique can be used to transport an integer number of electrons per cycle of the SAW frequency [26, 27, 92]. The number  $N$  of electrons per dot determines the dc current  $I = Nef$  through the constriction. The experiments

have demonstrated the quantization of the dc current at the values corresponding to integer  $N = 1..4$ . The robustness of the current quantization with respect to a range of parameters (gate voltage, bias voltage, amplitude of SAW) implies that the number of electrons in each quantum dot is a deterministic rather than stochastic quantity.

The quantized current can only be observed deep inside the pinch-off regime. The concentration  $n = N/\lambda_{SAW}$  of electrons in the pinch-off region, where  $\lambda_{SAW} \approx 1\mu\text{m}$  is the wavelength of the SAW, is much smaller than the concentration  $n_0 = 4/\lambda_F$  of electrons in the 2DEG, where  $\lambda_F \approx 50\text{ nm}$  is the Fermi wavelength. For this reason, the electrons in the constriction do not screen the electrostatic potential induced by the SAW. Moreover, the kinetic energy of electrons in moving quantum dots is very small, so that the Coulomb interaction is the dominant energy scale. The quantum dot that has just been formed near the entrance of the constriction can be considered as an electron box connected to the 2DEG reservoir. The Coulomb repulsion determines the number of electrons in the dot so that the free energy of the system is minimized. The number of electrons in the dot can be controlled by the gate voltage and by the amplitude of SAW (the increase of the SAW amplitude makes the potential minima deeper which has a similar effect as an increase of the gate voltage).

Due to the substantial difference between the velocity of the SAW,  $v_{SAW} \simeq 3 \times 10^3$  m/s, and the Fermi velocity,  $v_F \simeq 10^5$  m/s, the formation of new quantum dots occurs adiabatically. In contrast to a conventional electron box, the barrier between the quantum dot and the reservoir varies in time so that its transparency decreases by many orders of magnitude while electrons fill the quantum dot. The dynamics of this process is yet to be understood. An important parameter that determines the maximum operation frequency seems to be the time dependence of the transparency (or conductance) of the barrier that separates the most recently filled dot from the 2DEG.

The experimental observation of quantized currents at frequencies around 3 GHz suggests that electron transfer occurs through a low energy barrier, although the accuracy of the device may be determined by residual thermal or quantum transport through a high energy barrier. Finally we note that another physical mechanism which might negatively affect the accuracy - impurity scattering of the electrons in the moving quantum dots - becomes less effective with increasing driving frequency [27].

## 6.2 Phase locking of coherent Cooper pair tunneling

A current standard based on the tunneling of single Cooper pairs may be an interesting alternative for the single-electron pump. By using the Coulomb blockade state for Cooper pairs, one can take advantage of the coherence which is intrinsic to the superconducting state. However, achieving the Coulomb blockade for Cooper pairs is very difficult since the effect can be masked by either the onset of a supercurrent or by unwanted quasiparticle tunneling. Quasiparticle tunneling is presumably the main cause of the poor performance of Cooper pair pumps [13, 93].

Recently the blockade for Cooper pair tunneling was demonstrated in one-dimensional series arrays of small-capacitance tunnel junctions with tunable Josephson coupling [25]. In this system the charge is transferred by Cooper pairs *solitons* which can be considered as the dual analog of the vortices in a one-dimensional parallel Josephson array. In particular, the Coulomb blockade voltage corresponds to the threshold voltage at which Cooper pair solitons enter the array. In the absence of dissipation, the Cooper pair solitons are expected to propagate coherently through uniform arrays [94]. A word of caution is needed here.

In realistic arrays the propagation of Cooper pair solitons might be hindered due to the pinning by offset charges. The increase of the Josephson energy effectively reduces this pinning. On the other hand, at  $E_J \simeq E_C$  the onset of superconductivity occurs in the array, which destroys the Cooper pair solitons.

### 6.3 Electron counting by a high-speed electrometer

The single-electron current standards discussed so far are based on the *active* manipulation of electrons or Cooper pairs, in other words current generation techniques. A tempting alternative is to try to *passively* count individual charge quanta passing through a voltage biased one-dimensional array of tunnel junctions using a high-speed electrometer coupled to one of the islands of the array.

Due to correlations in the single-electron tunneling events, solitons of charge  $e$  (or  $2e$ ) will be running through the array. Mutual repulsion keeps the moving solitons at a certain average distance, so that the system of solitons is robust with respect to the random offset charges of the islands. Likharev et al. [87] have calculated the time evolution of the electric charge at an island of the array. In the frequency domain narrow peaks show up, positioned at frequency  $f = \langle I \rangle / e$ , where  $\langle I \rangle$  is the average current. If it possible to monitor these charge oscillations in time, one can actually realise an electron counter.

The main problem for the realisation of such an electron counter is to develop a charge detector with a high charge sensitivity in combination with a large bandwidth. Recently a promising step forward [40] has been made through the development of a radio frequency single-electron transistor (RF-SET). The working principle has already been described in Sec. 1.5.2. Possible error mechanisms in the electron counter based on RF-SET have yet to be analyzed.

## 7 Conclusions

We have reviewed the status of the understanding of single-electron devices in metrology. By pumping single electrons one can generate a current which is determined by the pump frequency and the fundamental electron charge. There are two possible routes for utilization of this idea. One route is to devise a high precision *current standard* based on the pumping principle. This would also allow for a comparison with a current measured on the basis of a Josephson voltage standard and a quantum Hall resistance standard. The direct comparison of the two currents would give a check of the internal consistency of the quantum standards. There are several technical difficulties in this, one of the main problems being the small currents (presently a few picoamperes) generated by single-electron pumps.

The second possible route is to realize a new *capacitance standard*, circumventing the cumbersome use of the calculable capacitor. The idea is to pump a known charge onto a capacitor and then to measure the resulting voltage. Note that this is a dc capacitance standard. In order to link its value to that of the calculable capacitor, which operates at 1592 Hz, more knowledge is required about the frequency dependence of these standards.

The state of the art 7-junction single-electron pump has an intrinsic error per pumped electron of 1 part in  $10^8$  [17], while generating a picoampere current. This approaches the level of metrological accuracy currently obtained for Josephson voltage standards and quantum Hall standards. However, the measured error rate is many orders of magnitude larger than that predicted by theory.

Although the quantum Hall effect is also not completely understood, it is an inherent quantum effect, whereas single-electron current generators are devices that have to be designed in order to *suppress* quantum mechanical effects (e.g. cotunneling). Furthermore, the quantized Hall resistance has been shown to be independent of material parameters, while single-electron generators are very sensitive to the design layout and choice of device parameters. For these reasons a detailed understanding of the physical mechanisms of errors is essential for the use in metrology, and future research is needed in this direction. Therefore, at this stage, the single-electron pumps cannot be considered as being at a similar level as the Josephson voltage standard or the quantum Hall standard, neither experimentally nor theoretically.

In this review, we have mainly concentrated on conventional tunnel junction SET devices such as pumps and turnstiles. Although the present accuracy is still not sufficient for all metrological applications, the ongoing technical developments justify the expectation of considerable improvements in device performance. For future designs several issues are important. For example to try waveforms which have been predicted to be much better than the triangular shape. Secondly, to minimize noise from charge traps in the substrate by alternative designs or materials. Also, the complexity of the design of turnstiles and pumps may be reduced by introducing high-ohmic microresistors in the bias leads thus suppressing cotunneling. In this way one could obtain an error per transferred electron equal to that of a 7-junction pump, but with less tunnel junctions. It makes the operation of the device easier and makes the device more robust.

In addition, there are promising candidates for alternative single-electron current standards. One example is the SAW device, another example is a single-electron counter based on a high-speed SET transistor.

A large worldwide research is evolving in the field of manipulation of single electron charges. The efforts give enough confidence in a future realisation of a high precision SET current standard.

## 8 Acknowledgments

We are indebted to A. Zorin and D. Haviland for their input to Secs. 3.5 and 6.2 and to M. Keller for suggestions and careful reading of the manuscript. We thank J. Martinis, H. D. Jensen, and A. Hartland for discussions. This work was supported by the EU (SETamp project, contract number SMT4-CT96-2049).

## References

- [\*] Present address: Niels Bohr Institute f. APG, Ørsted Laboratory, Universitetsparken 5, DK-2100 Copenhagen Ø
- [\*\*] Permanent address: Nuclear Physics Institute, Moscow State University, Moscow 119899 GSP, Russia.
- [1] H. R. Zeller and I. Giaver, *Phys. Rev.* **181**, 789 (1969).
- [2] T. A. Fulton and G. J. Dolan, *Phys. Rev. Lett.* **59**, 109 (1987).
- [3] D. V. Averin and K. K. Likharev, in *Mesoscopic Phenomena in solids*, edited by B. L. Al'tshuler, P. A. Lee, and R. A. Webb (Elsevier, Amsterdam, 1990).

- [4] P. Delsing, K. K. Likharev, L. S. Kuzmin, and T. Claeson, *Phys. Rev. Lett.* **63**, 1180 (1989).
- [5] Y. V. Nazarov, *Zh. Eksp. Teor. Fiz.* **95**, 975 (1989) [*Sov. Phys. JETP* **68**, 561 (1989)]; *Pis'ma Zh. Eksp. Teor. Fiz.* **49**, 1349 (1989) [*JETP Lett.* **49**, 126 (1989)].
- [6] M. H. Devoret *et al.*, *Phys. Rev. Lett.* **64**, 1824 (1990).
- [7] S. M. Girvin *et al.*, *Phys. Rev. Lett.* **64**, 3183 (1990).
- [8] K. Flensberg *et al.*, *Physica Scripta* **T42**, 189 (1992).
- [9] D. B. Haviland, Y. Pashkin, and L. S. Kuzmin, *Physica* **203**, 347 (1994).
- [10] L. S. Kuzmin *et al.*, *Phys. Rev. B* **54**, 10074 (1996).
- [11] W. Zheng *et al.*, *cond-mat/9806044*.
- [12] P. Delsing, K. K. Likharev, L. S. Kuzmin, and T. Claeson, *Phys. Rev. Lett.* **63**, 1861 (1989).
- [13] L. J. Geerligs *et al.*, *Phys. Rev. Lett.* **64**, 2691 (1990).
- [14] H. Pothier *et al.*, *Europhys. Lett.* **17**, 249 (1992).
- [15] J. M. Martinis, M. Nahum, and H. D. Jensen, *Phys. Rev. Lett.* **72**, 904 (1994).
- [16] M. W. Keller, J. M. Martinis, N. M. Zimmerman, and A. H. Steinbach, *Appl. Phys. Lett.* **69**, 1804 (1996).
- [17] M. W. Keller, J. M. Martinis, A. H. Steinbach, and N. M. Zimmerman, *IEEE Trans. Instrum. Meas.* **46**, 307 (1997).
- [18] M. W. Keller, J. M. Martinis, and R. L. Kautz, *Phys. Rev. Lett.* **80**, 4530 (1998).
- [19] E. R. Williams, R. N. Ghosh, and J. M. Martinis, *J. Res. Natl. Inst. Stand. Technol.* **97**, 299 (1992).
- [20] K. K. Likharev and A. Zorin, *J. Low. Temp. Phys* **59**, 347 (1985).
- [21] L. S. Kuzmin and D. B. Haviland, *Phys. Rev. Lett.* **67**, 2860 (1991).
- [22] L. S. Kuzmin and D. B. Haviland, *Physica Scripta* **T42**, 171 (1992).
- [23] Y. Nazarov and A. A. Odintsov, in *Single-electron tunneling and mesoscopic devices*, edited by H. Koch and H. Lübbig (Springer-Verlag, Berlin, 1992), p. 91.
- [24] L. S. Kuzmin, Y. Pashkin, A. Zorin, and T. Claeson, *Physica B* **203**, 376 (1994).
- [25] D. B. Haviland and P. Delsing, *Phys. Rev. B* **54**, R6857 (1996).
- [26] J. M. Shilton *et al.*, *J. Phys.: Condens. Matter* **8**, L531 (1996).
- [27] V. I. Talyanskii *et al.*, *Phys. Rev. B* **56**, 15180 (1997).
- [28] N. M. Zimmerman, J. L. Cobb, and A. F. Clark, *IEEE Trans. Instrum. Meas.* **46**, 294 (1997).

- [29] M. W. Keller, private communication.
- [30] B.N. Taylor and T.J. Witt, *Metrologia* **26**, 47 (1989).
- [31] *Single Charge Tunneling*, edited by H. Grabert and M. Devoret, Nato ASI Series B Vol. 294 (Plenum Press, New York), 1992.
- [32] P. Lafarge *et al.*, *Z. Phys. B* **85**, 327 (1991).
- [33] T. A. Fulton, P. L. Gammel, and L. N. Dunkleberger, *Phys. Rev. Lett.* **67**, 3148 (1991).
- [34] A.F. Clark *et al.*, *Appl. Phys. Lett.* **66**, 2588 (1995).
- [35] M.J. Yoo *et al.*, *Science* **276**, 579 (1997).
- [36] A. N. Korotkov, M. R. Samuelsen and S. A. Vasenko, *Journal of Applied Physics* **76**, 3623 (1994).
- [37] C. Liu and Q. Niu, *Physics Reports* **286**, 349 (1997).
- [38] M. Field *et al.*, *Phys. Rev. Lett* **77**, 350 (1996).
- [39] Y. Y. Wei, J. Weiss, K. von Klitzing, and K. Eberl, *Appl. Phys. Lett.* **71**, 2514 (1997).
- [40] R. J. Schoelkopf *et al.*, *Science* **280**, 1238 (1998).
- [41] J. P. Pekola, K. P. Hirvi, J. P. Kauppinen, and M. A. Paalanen, *Phys. Rev. Lett.* **73**, 2903 (1994).
- [42] S. Farhangfar *et al.*, *J. Low Temp. Phys.* **108**, 191 (1997).
- [43] L. I. Glazman and K. A. Matveev, *Pis'ma Zh. Eksp. Teor. Fiz.* **48**, 403 (1988) [*JETP Lett.* **48**, 445 (1988)].
- [44] D. V. Averin and A. N. Korotkov, *zh. Eksp. Teor. Fiz.* **97**, 1661 (1990) [*Sov. Phys. JETP* **90**, 937 (1990)].
- [45] C. W. J. Beenakker, *Phys. Rev. B* **44**, 1646 (1991).
- [46] V. F. Anderegg *et al.*, *Physica B* **165-166**, 61 (1990).
- [47] L. P. Kouwenhoven *et al.*, *Z. Phys. B – Condensed Matter* **85**, 367 (1991).
- [48] C. Urbina *et al.*, *IEEE Trans. Magn.* **27**, 2578 (1991).
- [49] S. Verbrugh, ph.D. thesis, Delft University of Technology.
- [50] H. D. Jensen and J. M. Martinis, *Phys. Rev. B* **46**, 13407 (1992).
- [51] H. Pothier, Ph.D. thesis, University of Paris 6, 1991.
- [52] A. Iwasa, A. Fukushima, and A. A. Odintsov, *Jpn. J. Appl. Phys.* **34**, 5871 (1995).
- [53] L. R. C. Fonseca, A. N. Korotkov, and K. K. Likharev, *Appl. Phys. Lett.* **69**, 1858 (1996).

- [54] L. R. C. Fonseca, A. N. Korotkov, and K. K. Likharev, *J. Appl. Phys.* **79**, 9155 (1996).
- [55] D. V. Averin and A. A. Odintsov, *Phys. Lett. A* **140**, 251 (1989).
- [56] D. V. Averin and Y. V. Nazarov, *Phys. Rev. Lett.* **65**, 2446 (1990).
- [57] T. M. Eiles, G. Zimmerli, H. D. Jensen, and J. M. Martinis, *Phys. Rev. Lett.* **69**, 148 (1992).
- [58] C. Pasquier *et al.*, *Phys. Rev. Lett.* **70**, 69 (1993).
- [59] D. J. Paul, J. Cleaver, H. Ahmed, and T. Whall, *Phys. Rev. B* **49**, 16514 (1994).
- [60] H. Matsuoka and S. Kimura, *Appl. Phys. Lett.* **66**, 613 (1995).
- [61] A. N. Korotkov, D. V. Averin, K. K. Likharev, and S. A. Vasenko, in *Single-electron tunneling and mesoscopic devices*, edited by H. Koch and H. Lübbig (Springer-Verlag, Berlin, 1992).
- [62] Y. V. Nazarov, *J. Low Temp. Phys.* **90**, 77 (1993).
- [63] D. V. Averin, *Physica B* **194-196**, 979 (1994).
- [64] K. Flensberg, *Phys. Rev. B* **55**, 113118 (1997).
- [65] L. J. Geerligs and M. M. J. E. Mooij, *Physica B* **194-196**, 1267 (1994).
- [66] J. König, H. Schoeller, and G. Schön, *Phys. Rev. Lett.* **78**, 4482 (1997).
- [67] P. Joyez *et al.*, *Phys. Rev. Lett* **79**, 1349 (1997).
- [68] P. Lafarge and D. Esteve, *Phys. Rev. B* **49**, 13309 (1993).
- [69] A.A. Odintsov, V. Bujanja, and G. Schön, *Phys. Rev. B* **46**, 6875 (1992).
- [70] A. Zorin, private communication.
- [71] J. M. Martinis and M. Nahum, *Phys. Rev. B* **48**, 18316 (1993).
- [72] J. M. Martinis, M. H. Devoret, and J. Clarke, *Phys. Rev. B* **35**, 4682 (1987).
- [73] D. Vion *et al.*, *J. Appl. Phys.* **77**, 2519 (1995).
- [74] A. B. Zorin, *Rev. Sci. Instrum.* **66**, 4296 (1995); D. C. Glatli *et al.*, *J. Appl. Phys.* **81**, 7350 (1997).
- [75] V. Bouchiat, ph.D. thesis, University of Paris 6, 1997, Ch.5.
- [76] G. Zimmerli, T. M. Eiles, R. L. Kautz, and J. M. Martinis, *Appl. Phys. Lett.* **61**, 237 (1992).
- [77] A. B. Zorin *et al.*, *Phys. Rev. B* **53**, 13682 (1996).
- [78] E. H. Visscher *et al.*, *Appl. Phys. Lett.* **66**, 305 (1995).

- [79] V. A. Krupenin, D. E. Presnov, M. N. Savvateev, H. Scherer, A. B. Zorin and J. Niemeyer, Conference on Precision Electromagnetic Measurements CPEM 1998, Conference Digest, ed. by T. L. Nelson, p. 140.
- [80] V. A. Krupenin, D. E. Presnov, M. N. Savvateev, H. Scherer, A. B. Zorin and J. Niemeyer, J. Appl. Phys, in press.
- [81] A. J. Manninen and J. P. Pekola, Czech. J. Phys. **46**, 2293 (1996).
- [82] I. O. Kulik and R. I. Shekter, Sov. Phys. JETP **41**, 308 (1975).
- [83] For general information about the nanostructure simulators use <http://web-ext2.darpa.mil/ETO/ULTRA/Modeling.html>.
- [84] R. H. Chen. MOSES: A general Monte Carlo simulator for single-electronic circuits. In Meeting Abstracts, volume 96-2, page 576. The Electrochemical Society, October 1996. For info about MOSES software package use <ftp://hana.physics.sunysb.edu/pub/moses/>.
- [85] L. R. C. Fonseca, A. N. Korotkov, K. K. Likharev, and A. A. Odintsov, J. Appl. Phys. **78**, 3238 (1995).
- [86] C. Wasshuber, H. Kosina, Superlatt. Microstr., **21**, No.1, 37 (1997); C. Wasshuber, *About Single-Electron Devices and Circuits*, Ph.D. Thesis, Institute for Microelectronics, University of Vienna, Austria, 1997, <http://a63.iue.tuwien.ac.at/diss/wasshuber/diss/diss.html>; For info about SIMON software package use <http://members.magnet.at/catsmeow/>.
- [87] N. S. Bakhvalov, G. S. Kazacha, K. K. Likharev, and S. I. Serdyukova. Sov. Phys. JETP, **68**, 581-587 (1989); K. K. Likharev, N. S. Bakhvalov, G. S. Kazacha, and S. I. Serdyukova, IEEE Trans. Magn. **25**, 1436 (1989).
- [88] M. Kirihara, N. Kuwamura, K. Taniguchi, and C. Hamaguchi, Extended Abstracts of the International Conference on Solid State Devices and Materials, pp. 328-330, Yokohama, Japan 1994.
- [89] S.A. Roy, *Simulation Tools for the Analysis of Single Electronic Systems*, PhD thesis, University of Glasgow, 1994.
- [90] D. V. Averin, A. A. Odintsov, and S. V. Vyshenskii, J. Appl. Phys. **73**, 1297 (1993).
- [91] R. Bauerschmitt and Y. V. Nazarov, Phys. Rev. B **47**, 9997 (1993).
- [92] J. M. Shilton *et al.*, J. Phys.: Condens. Matter **8**, L337 (1996).
- [93] L. J. Geerligs, *et al.*, Z. Phys. B **85**, 349 (1991).
- [94] A. A. Odintsov, Sov. Phys. JETP Lett. **60**, 738 (1994).